Youngstown MTBE Release Analysis and Pumping Recommendations

Cormac Rankin

05/06/2024

Contents

Problem Statement

The city of Youngstown experienced an MTBE release from a leaking gas station storage tank in the vicinity of several pumping wells. The MTBE release took place from June 1, 2017 until June 1, 2018. The nearby pumping wells are at risk of contamination by MTBE. A model must be developed to determine a pumping scheme which keeps the drinking water of Youngstown safe from MTBE over the time period of June 1, 2024 until December 31, 2039. All available data used in the analysis can be found in Appendix A.

Conceptual Model of Flow and Transport

The aquifer is bounded below by bedrock, but there is no bounding layer above. Therefore, the aquifer is unconfined as direct recharge from precipitation and surface runoff reaches the

aquifer. In this model, isotropy will be assumed because there is no information to indicate anisotropy. The site is also heterogeneous as different wells have different surrounding lithology (see figure 1A in Appendix A). This study site is far from any natural hydrologic boundaries. The flow and transport conditions of the site vary in time; this is clear from the tables and plots which show head values that change as a function of time. See table 1A in Appendix A for evidence that the head at the well locations changes with different dates. The primary direction of horizontal groundwater flow and transport is 160° clockwise from north, estimated first from the hand-drawn water table maps below. Water sources to the aquifer include precipitation and runoff which become groundwater recharge, while sinks are the pumping wells. The pumping wells 1-8 and 11 are the primary sinks of the aquifer. In the future, all pumping wells (wells 1-17) could be pumping, so these are also potential sinks. The only source of MTBE into the aquifer is the gas station, which released approximately 6 L/d (4.4 kg/d) of MTBE into the upper aquifer from June 1, 2017 to June 1, 2018. The sinks of MTBE are the pumping wells, which may draw MTBE from the aquifer along with the water.

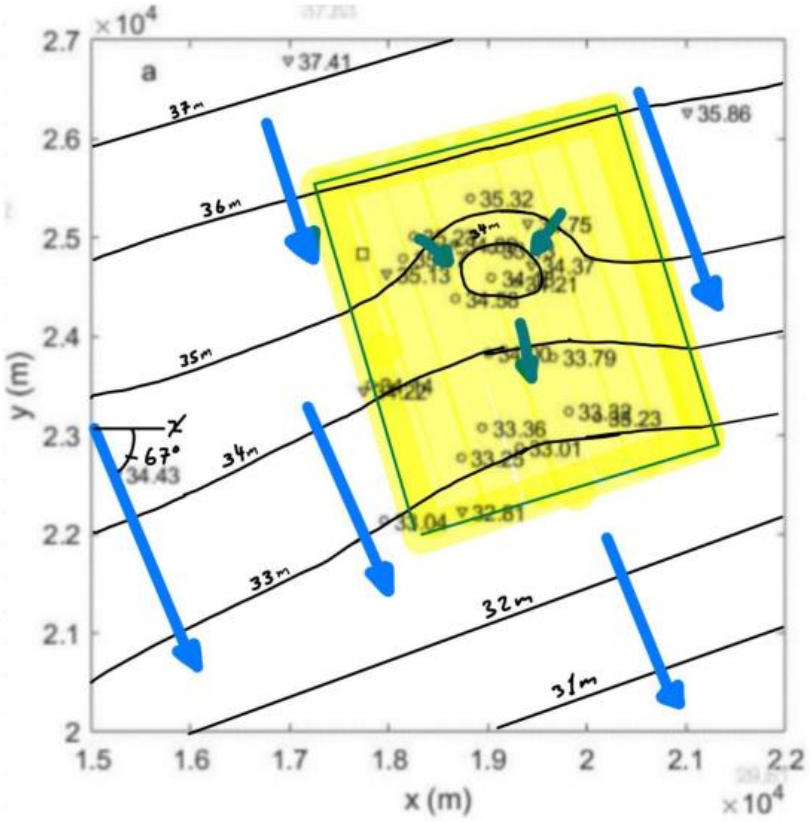

Figure 1. Head (m) at each pumping well and monitoring well in 2009 in site area with hand drawn head contours at one-meter intervals. Region affected by pumping is highlighted with arrows indicating the flow direction. Flow direction is -67° (South East).

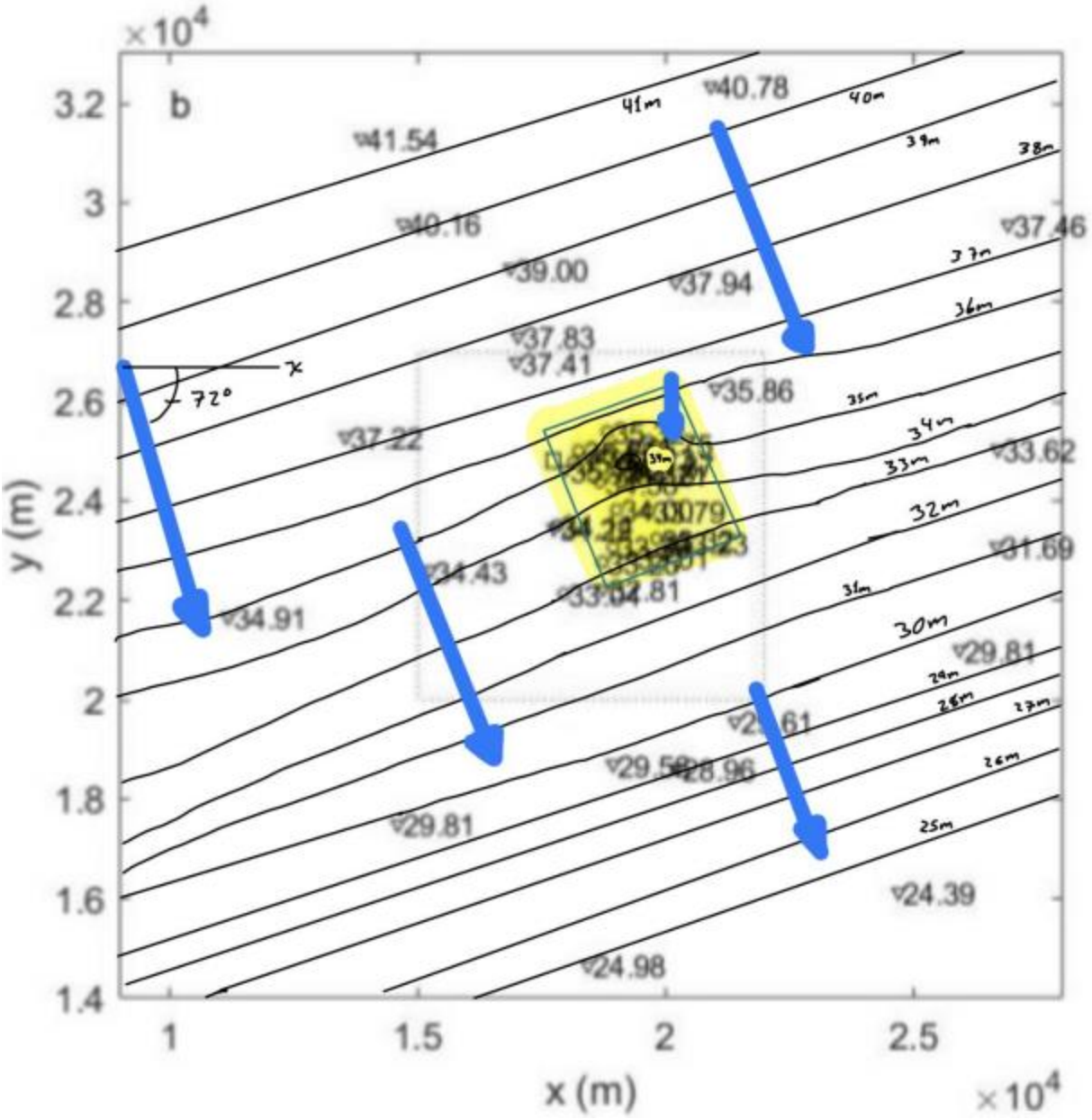

Figure 2. Head (m) at each pumping well and monitoring well in 2009 in entire region with hand-drawn head contours at one meter intervals. Region affected by pumping is highlighted and arrows indicating the flow direction are shown. Flow direction is -72° (South East).

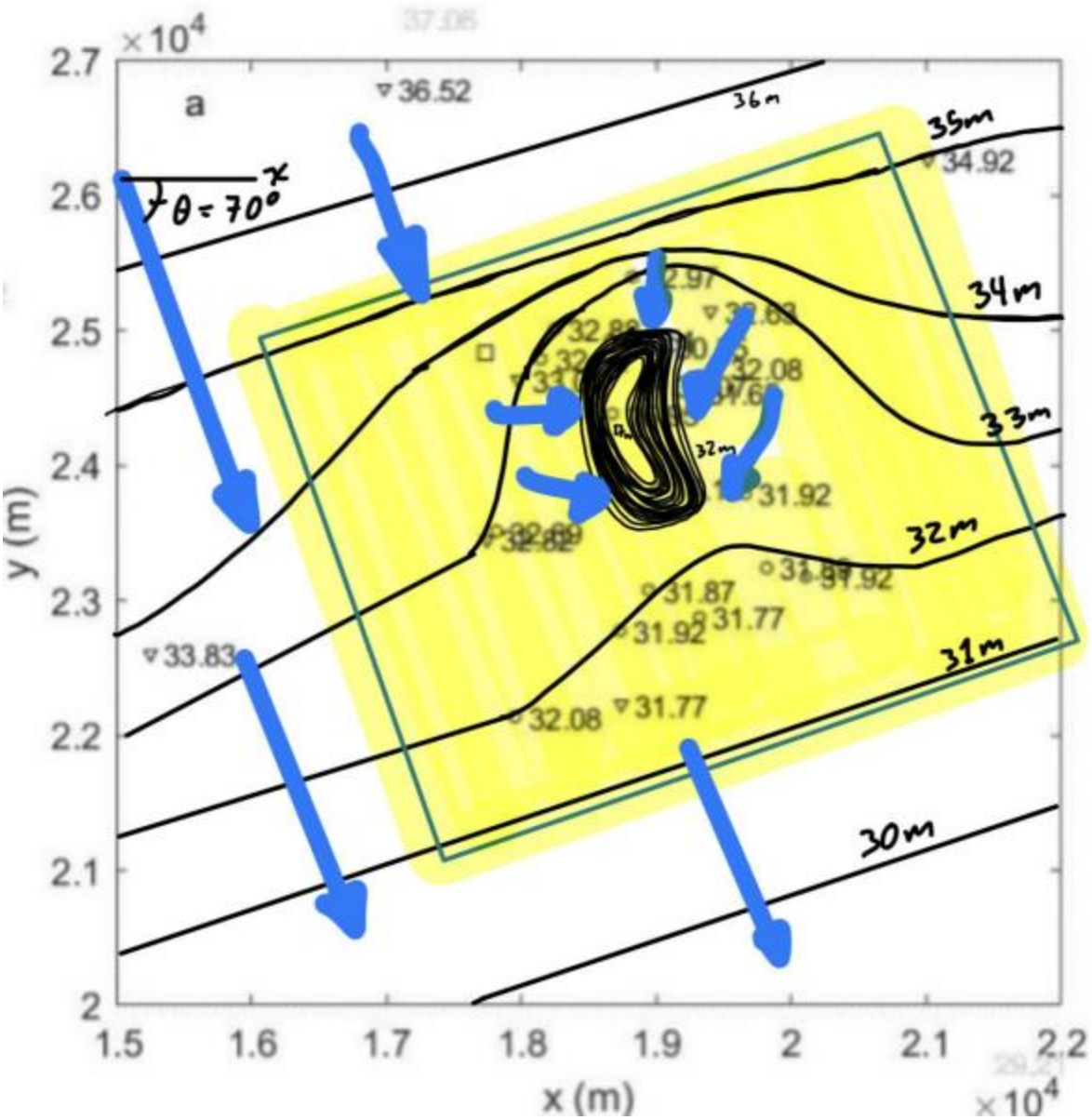

Figure 3. Head (m) at each pumping well and monitoring well in 2023 in site area with hand drawn head contours at one-meter intervals. Region affected by pumping is highlighted and arrows indicating the flow direction are shown. Flow direction is -70° (South East).

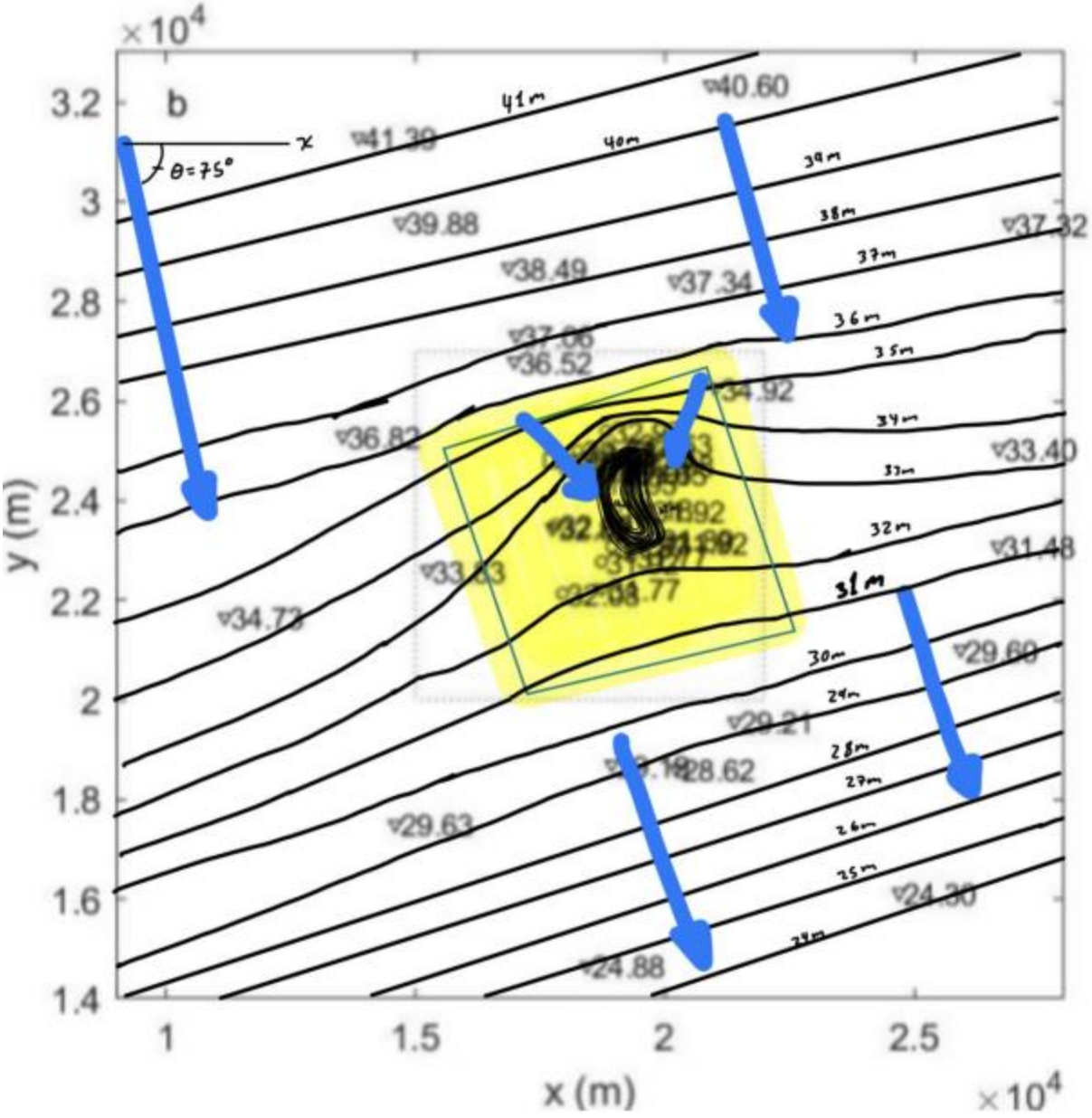

Figure 4. Head (m) at each pumping well and monitoring well in 2023 in entire region with hand-drawn head contours at one-meter intervals. Region affected by pumping is highlighted and arrows indicating the flow direction are shown. Flow direction is -75° (South East).

Mathematical Model of Flow and Transport

The mathematical models for groundwater flow in each layer of the aquifer are

$$S_y(\mathbf{x})\frac{\partial h_1}{\partial t} = \frac{\partial}{\partial x}\left(K(\mathbf{x})(h_1-\zeta)\frac{\partial h_1}{\partial x}\right) + \frac{\partial}{\partial y}\left(K(\mathbf{x})(h_1-\zeta)\frac{\partial h_1}{\partial y}\right) + N - \frac{K(\mathbf{x})}{\Delta b_{1,2}}(h_1-h_2) \quad (1)$$

for layer 1 which ranges from z = 19.69 meters to the top of the aquifer (39.5 meters)

$$S_2(\mathbf{x})\frac{\partial h_2}{\partial t} = \frac{\partial}{\partial x}\left(T_2(\mathbf{x})\frac{\partial h_2}{\partial x}\right) + \frac{\partial}{\partial y}\left(T_2(\mathbf{x})\frac{\partial h_2}{\partial y}\right) - \frac{K(\mathbf{x})}{\Delta b_{2,3}}(h_2-h_3) + \frac{K(\mathbf{x})}{\Delta b_{1,2}}(h_1-h_2) \quad (2)$$

for layer 2 which ranges from z = 6.48 meters to 19.69 meters

$$S_3(\mathbf{x})\frac{\partial h_3}{\partial t} = \frac{\partial}{\partial x}\left(T_3(\mathbf{x})\frac{\partial h_3}{\partial x}\right) + \frac{\partial}{\partial y}\left(T_3(\mathbf{x})\frac{\partial h_3}{\partial y}\right) + \frac{K(\mathbf{x})}{\Delta b_{2,3}}(h_2-h_3) - \sum_{i=1}^{17} Q_i(t)\delta(x-x_{w,i})\delta(y-y_{w,i}) \quad (3)$$

for layer 3, which ranges from z = -11.30 meters to 6.48 meters.

where $K(\boldsymbol{x})$ is the hydraulic conductivity as a function of the horizontal location, $h_1(\boldsymbol{x},t)$ is the head in the first layer of the aquifer and depends on space and time, ζ is the bottom elevation of the first layer of the aquifer, N is the recharge rate, $\Delta b_{a,b}$ is the vertical distance between the midpoints of layers a and b, Q_i is the pumping rate of well i, x and y are the spatial coordinates, $x_{w,i}$ is the location of well i in x dimension of the horizontal plane, $y_{w,i}$ is the location of well i in the y dimension of the horizontal plane, $T_2(\mathbf{x})$ is the transmissivity as a function of the horizontal location in layer 2, $T_3(\mathbf{x})$ is the transmissivity as a function of the horizontal location in layer 3, h_2 is the head in the second layer of the aquifer and depends on space and time, h_3 is the head in the third layer of the aquifer and depends on space and time, and $\mathbf{x} = (x,y)$ is the spatial coordinate. $S_2(\mathbf{x})$ is the storage coefficient for layer 2 and is a function of space and time, $S_3(\mathbf{x})$ is the storage coefficient for layer 2 and is a function of space and time.

Boundary Conditions for all layers are

$$h_k(\boldsymbol{x},t) = h_b(\boldsymbol{x}) \text{ at } \Gamma \quad (4)$$

where $h_b(\boldsymbol{x})$ is the head at the boundary, and Γ is the location of the boundary. Initial Conditions are

$$h_k(\boldsymbol{x}, t=0) = h_{k,0}(\boldsymbol{x}) \quad (5)$$

where $h_{k,0}$ is the solution to equations 1, 2, and 3, when the left side of these equations is set equal to zero (steady state), and only wells 1 and 11 are pumping at rates of 3,120 m^3/day and 215 m^3/day, respectively.

The governing equation for MTBE transport in the aquifer is given by

$$n\frac{\partial C}{\partial t} = \frac{\dot{M(t)}}{h_1 - \zeta}\delta(\mathbf{x} - \mathbf{x}_T) + \nabla \cdot [n\boldsymbol{D}\nabla \mathrm{C}] - \nabla \cdot (n\mathbf{v}\mathrm{C}) - \sum_{i=1}^{17}\frac{Q_i C}{\Delta z}\delta(\mathbf{x} - \mathbf{x}_{wi}) \quad (6)$$

where $\mathbf{x} = (x, y)$ is the spatial coordinate, $K(\mathbf{x})$ is hydraulic conductivity, h_1 is the head in layer 1, $\dot{M}$ is the mass loading rate (in units of mass per time), n is the porosity, $\mathbf{x}_T$ is the location of the source (the gas station), Q_i is the pumping rate of well i, $\mathbf{x}_{wi}$ is the location of well i, Δz is the model layer thickness in layer 3, δ is the dirac delta function, $C = C(x, y, z, t)$ is concentration as a function of position and time, and $\mathbf{v}$ is the groundwater velocity vector given by

$$\boldsymbol{v} = -\frac{K(\mathbf{x})}{n}\nabla h \quad (7)$$

and $\boldsymbol{D}$ is the dispersion tensor given by

$$D_{xx} = \alpha_L \frac{{v_x}^2}{|\boldsymbol{v}|} + \alpha_{TH}\frac{{v_y}^2}{|\boldsymbol{v}|} + \alpha_{TV}\frac{{v_z}^2}{|\boldsymbol{v}|} \quad (8)$$

$$D_{xy} = D_{yx} = (\alpha_L - \alpha_{TH})\frac{v_x v_y}{|\boldsymbol{v}|} \quad (9)$$

$$D_{yy} = \alpha_L \frac{{v_y}^2}{|\boldsymbol{v}|} + \alpha_{TH}\frac{{v_x}^2}{|\boldsymbol{v}|} + \alpha_{TV}\frac{{v_z}^2}{|\boldsymbol{v}|} \quad (10)$$

$$D_{zz} = \alpha_L \frac{{v_z}^2}{|\boldsymbol{v}|} + \alpha_{TV}\frac{{v_x}^2}{|\boldsymbol{v}|} + \alpha_{TV}\frac{{v_y}^2}{|\boldsymbol{v}|} \quad (11)$$

$$D_{xz} = D_{zx} = (\alpha_L - \alpha_{TV})\frac{v_x v_z}{|\boldsymbol{v}|} \quad (12)$$

$$D_{yz} = D_{zy} = (\alpha_L - \alpha_{TV})\frac{v_y v_z}{|\boldsymbol{v}|} \quad (13)$$

where α_L and α_{TH} are the longitudinal and horizontal transverse dispersivities, respectively, α_{TV} is the vertical transverse dispersivity, v_x is the x component of the velocity vector, v_y is the y component of the velocity vector, v_z is the z component of the velocity vector, and $|\mathbf{v}|$ is the magnitude of the velocity vector. The initial and boundary conditions are

$$C(x, y, z, 0) = 0 \quad (14)$$

$$\nabla C \cdot \boldsymbol{n} = 0 \text{ at all boundaries} \quad (15)$$

where $\mathbf{n}$ is the outward unit normal vector.

Numerical Formulation: Horizontal and Vertical Discretization, Hydraulic Conductivity Distribution

MODFLOW is used to model flow in the aquifer domain, and MT3D-USGS is used to model transport of MTBE in the simulation.

The grid is oriented at 20 degrees clockwise, where zero degrees is east. The coordinates of the upper left corner of the grid are 14500 meters in the x dimension and 25000 meters in the y dimension. The length of sides oriented in the direction of flow is 4,875 meters (the blue boundary line in Figure 7 below). The length of the sides transverse to the flow direction is 5,625 meters (the green boundary line in Figure 7 below). The horizontal discretization of the domain varies in space (see figure 6), with grid cells ranging from a size of 40 m X 100 m near the boundaries to a size of 100 m X 100 m in the middle of the grid. Boundaries in the direction of flow are 65 grid boxes long and boundaries transverse to flow are 75 grid boxes long. The grid selected is optimal for this model because it encompasses the extent of the head influenced by well pumping, and at its boundaries the head contours are mostly unaffected by the pumping, as evidenced by figure 5 below. Therefore, this domain encompasses the region of interest without including extraneous information that will slow the model. The selected horizontal discretization balances accuracy with computation time, a discretization larger than 100 would sacrifice accuracy, while a very fine discretization would be too slow, 75 meters is a good middle value.

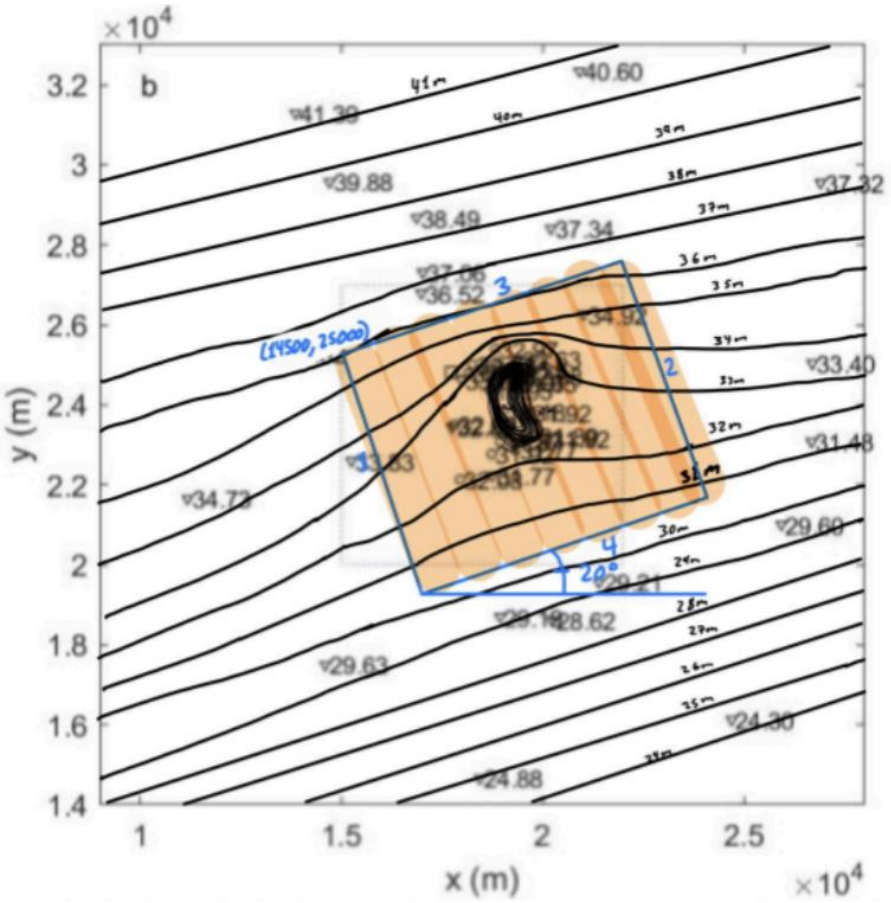

Figure 5. Sketch of the horizontal extend of the domain on water table map with head contours (m) at an interval of one meter. Horizontal axis is the x coordinate in meters, vertical axis is the y coordinate in meters.

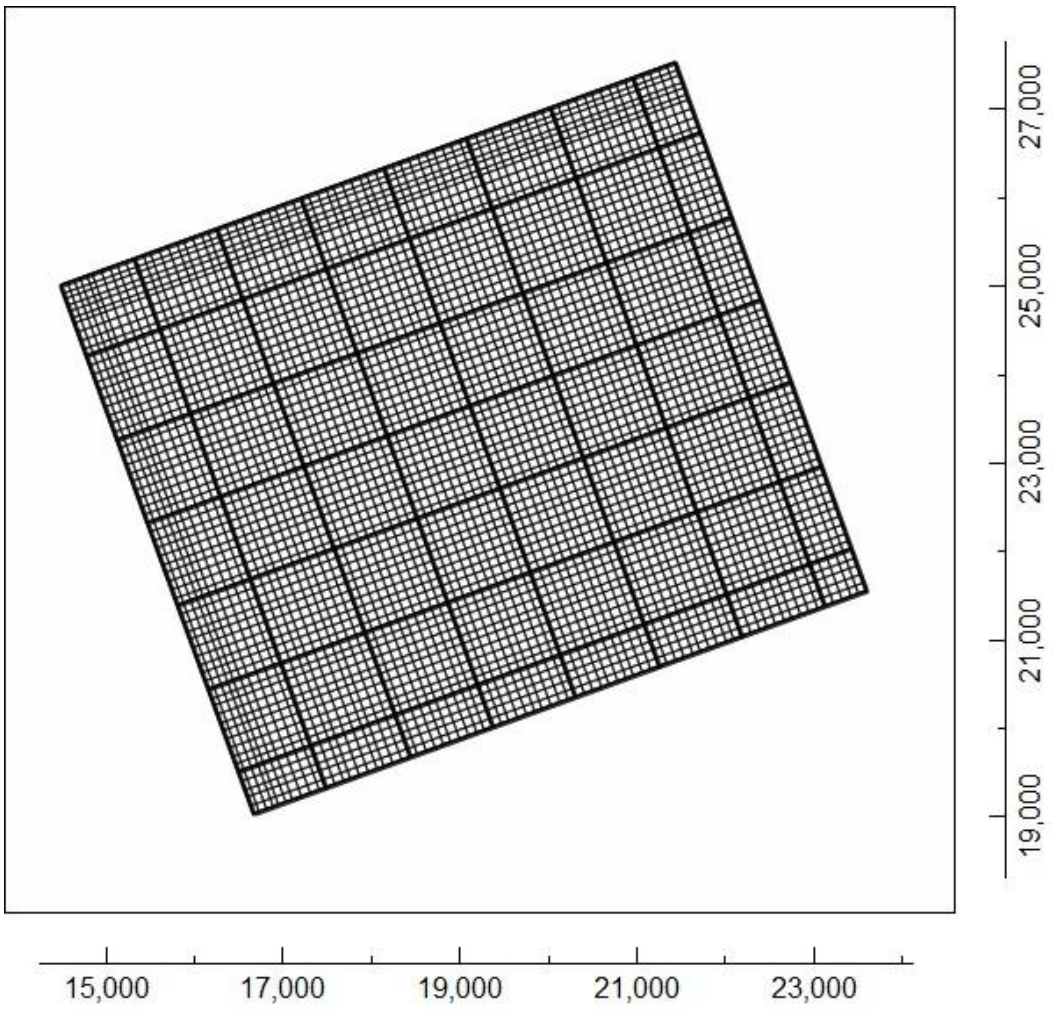

Figure 6. Image of the horizontal extent of the domain and domain grid on water table map in Modelmuse. Horizontal axis is the x coordinate in meters, and the vertical axis is the y coordinate in meters.

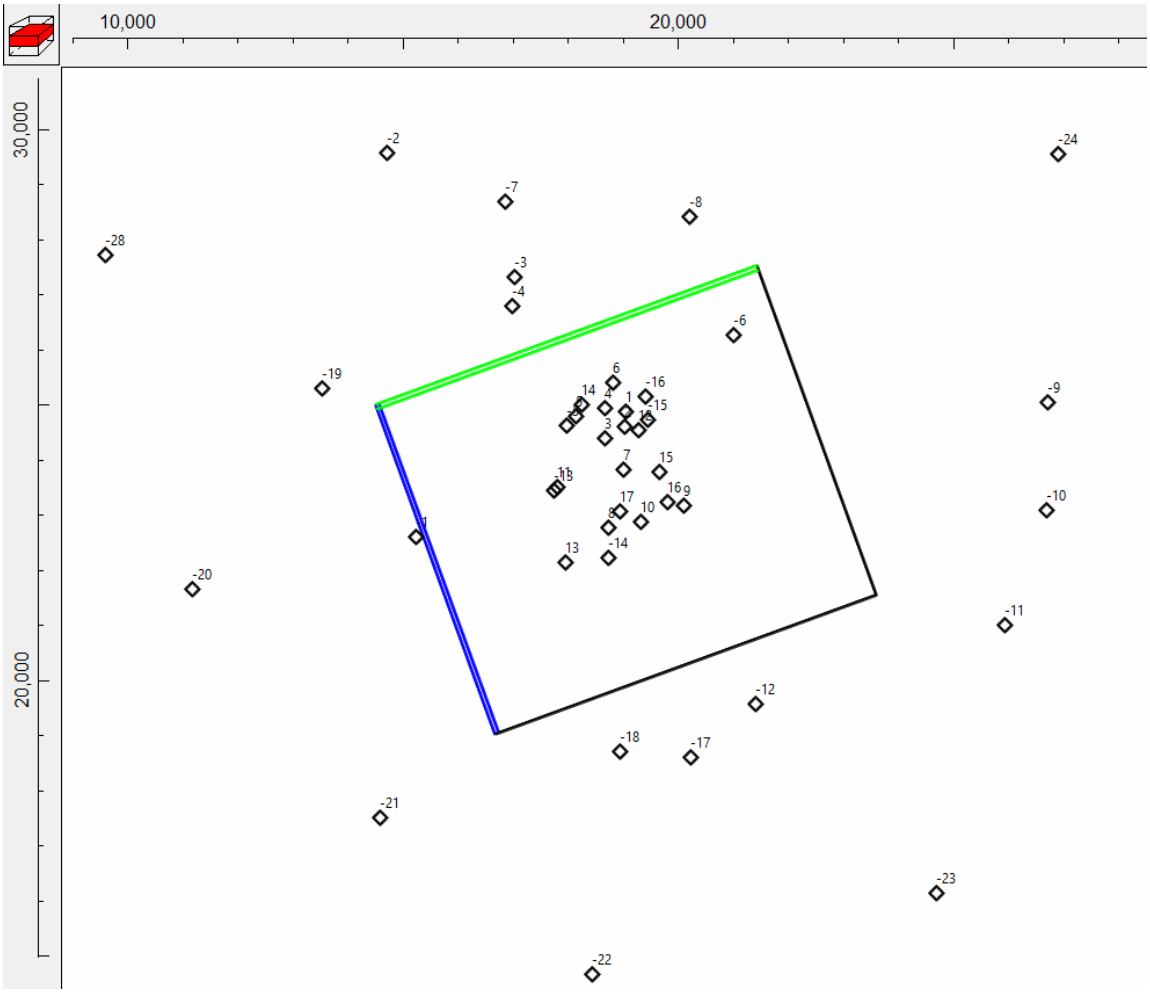

Figure 7. Image of the horizontal extent of the domain on water table map in ModelMuse. Horizontal axis is the x coordinate in meters, and the vertical axis is the y coordinate in meters. Monitoring wells are differentiated by pumping wells as their labels contain a "-" before the well number.

Vertical discretization was based on the pumping wells and associated elevations, not the monitoring wells. The top of layer one represents the maximum value of the ground surface (39.50 meters), while the bottom of layer three represents the minimum elevation of the top of bedrock (-11.30 meters), refer to table 2A in Appendix A for these elevations. The top of layer three was chosen such that layer three encompasses the entirety of all of the well screens. According to Table Two below, the highest-elevation top of well screen is 6.5 meters. Layer one should contain the water table at the model boundaries. A bottom elevation of 20 meters for layer one contains the water table at the boundaries. Water table elevation equals head in this case so refer figure 5 above for the rough head values at the boundaries. A vertical discretization of three layers was chosen because a higher vertical discretization would be unnecessary for this analysis and slow down the model.

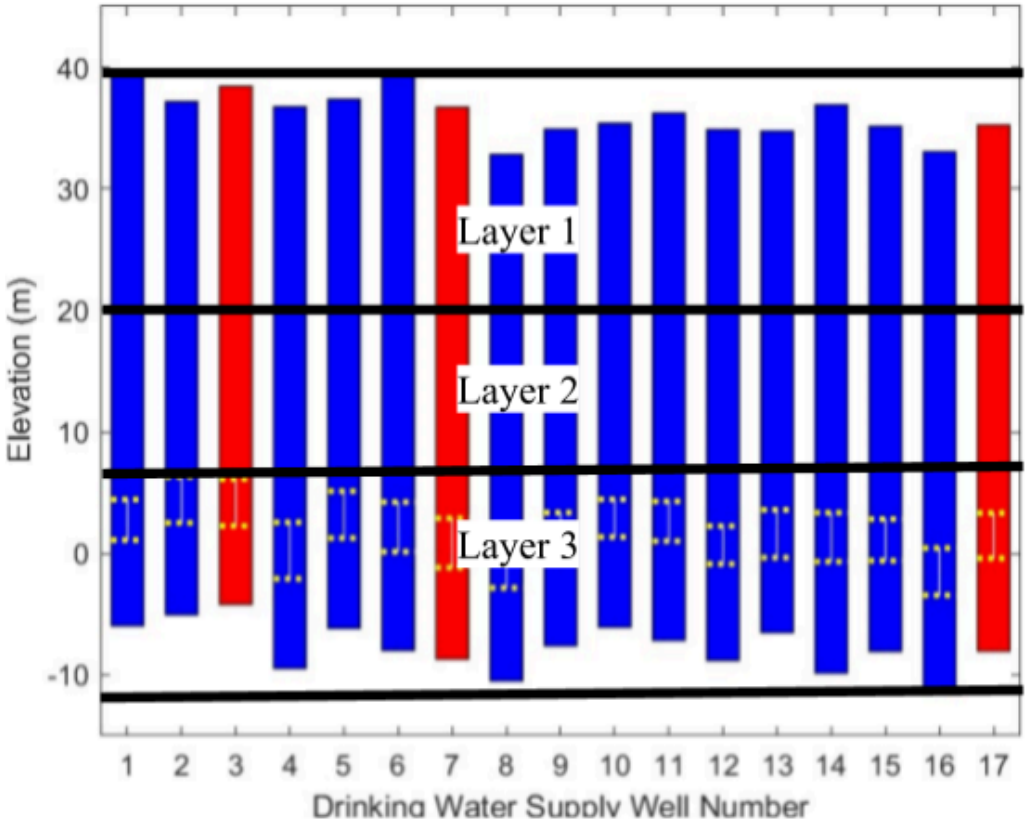

Figure 8. Sketch of vertical discretization based on the lithology of pumping wells. Vertical axis denotes elevation above sea level. Pumping well numbers are shown across the bottom. Blue shading represents medium sand and red shading represents sandy loam. The screened interval is denoted by a thin vertical line. The top and bottom of the screened intervals are denoted by thick dashed lines.

The site is composed of both sandy loam and medium sand. The exact location of the sandy loam is not known, but is estimated in the model based on well lithology in figure 1A in Appendix A

(or see figure 8 above). The figure below displays the chosen sandy loam and medium sand distribution in the model domain. This distribution of soil types is appropriate as it is consistent with available data, but there is a large amount of uncertainty in the exact boundary of the sandy loam.

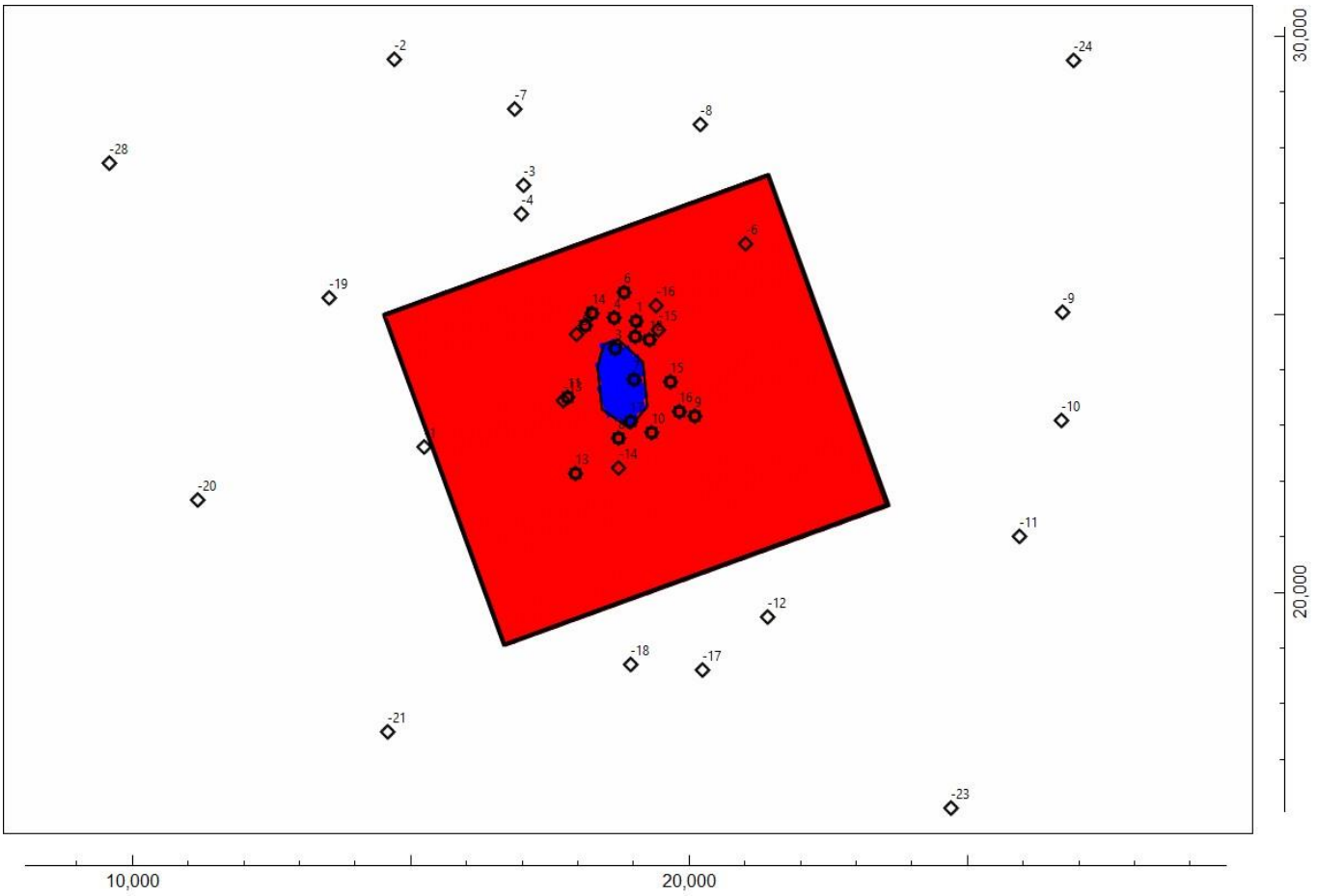

Figure 8. Color grid showing the medium sand aquifer in red and the sandy loam in blue. The horizontal axis is the x coordinate in meters and the vertical axis is the y coordinate in meters. Monitoring wells are denoted with a "-" before the well number.

Numerical Formulation: Parameter Values, Temporal Discretization, Boundary Heads, Initial Flow Conditions, and Peclet Number Discussion

The values of the parameters in the mathematical model are shown in the table below.

Table 1. Numerical Parameter Values

Specific Yield, Sandy Loam ($S_{y,\,loam}$)	0.150	
Specific Yield, Medium Sand ($S_{y,\,sand}$)	0.525	
Hydraulic Conductivity, Sandy Loam ($K_{x,\,loam}$)	2.31	m/d
Hydraulic Conductivity, Medium Sand ($K_{x,\,sand}$)	23.45	m/d
Specific Storage, Sandy Loam ($S_{s,\,loam}$)	0.00000999	m^{-1}
Specific Storage, Medium Sand ($S_{s,\,sand}$)	0.0000131	m^{-1}
Transmissivity Layer 2, Sandy Loam ($T_{2,\,Loam}$)	30.5	m^2/d
Transmissivity Layer 2, Medium Sand ($T_{2,\,sand}$)	310	m^2/d
Transmissivity Layer 3, Sandy Loam ($T_{3,\,Loam}$)	41.1	m^2/d
Transmissivity Layer 3, Medium Sand ($T_{3,\,sand}$)	417	m^2/d
Storage coefficient Layer 2, Sandy Loam ($S_{2,\,loam}$)	0.000132	
Storage coefficient Layer 2, Medium Sand ($S_{2,\,sand}$)	0.000173	
Storage coefficient Layer 3, Sandy Loam ($S_{3,\,loam}$)	0.000178	
Storage coefficient Layer 3, Medium Sand ($S_{3,\,sand}$)	0.000233	
Thickness of Layer 2 (b_2)	13.2	m
Thickness of Layer 3 (b_3)	17.8	m
Vertical distance between layers 1 and 2 ($b_{1,2}$)	16.5	m
Vertical distance between layers 2 and 3 ($b_{2,3}$)	16.0	m
Recharge Rate (N)	0.013	m/year
Pumping Rates and Well Locations	See Table 2	
Porosity	0.2	m
Horizontal Transverse Dispersivity (α_{TH})	5.25	m
Longitudinal Dispersivity (α_L)	52.5	m
Vertical Transverse Dispersivity (α_{TV})	2.63	m
Mass Loading Rate, ($\dot{M}_1$), from June 1, 2017 to June 1, 2018	4.40	kg/day
Mass Loading Rate, all other times ($\dot{M}_2$)	0	kg/day
Source Location (X_T)	(17740, 24830)	m
Δz	17.8	m

In table 1 above, transmissivity was calculated as $K(\mathbf{x})b_k$ and the storage coefficient is calculated with the equation $S_s(\mathbf{x})b_k$, where b_k is the thickness of a given layer *k*.

Table 2. Well Pumping Information

Pumping rates for periods 2-4 are based on information from table 2A in Appendix A

Well ID	x Coordinate (m)	y Coordinate (m)	Head 2009 (m)	Pumping Rate, Time Period 1 (m^3/d)	Pumping Rate, Time Period 2 (m^3/d)	Pumping Rate, Time Period 3 (m^3/d)	Pumping Rate Time Period 4 (m^3/d)	Pumping Rate, Time Period 5 (m^3/d)
				April 30, 2009	May 1, 2009 - June 1, 2017	June 1, 2017 - June 1, 2018	June 1, 2018 - June 1, 2024	June 1, 2024 - December 31, 2039
PW1	19042	24881	33.12	3120	3120	3120	3120	0
PW2	19035	24597	34.25	0	2120	2120	2120	0
PW3	18672	24384	34.5	0	1460	1460	1460	0
PW4	18664	24932	34.83	0	1780	1780	1780	0
PW5	18145	24788	35.08	0	980	980	980	0
PW6	18825	25399	35.29	0	520	520	520	2000
PW7	19008	23829	34	0	1470	1470	1470	0
PW8	18733	22774	33.32	0	180	180	180	0
PW9	20109	23175	33.29	0	0	0	0	2000
PW10	19321	22876	33.23	0	0	0	0	0
PW11	17814	23513	34.06	215	215	215	215	250
PW12	19280	24543	34.21	0	0	0	0	0
PW13	17953	22136	33.05	0	0	0	0	3500
PW14	18249	25013	35.16	0	0	0	0	0
PW15	19660	23790	33.8	0	0	0	0	1845
PW16	19818	23241	33.39	0	0	0	0	2000
PW17	18943	23076	33.46	0	0	0	0	250
Total Pumping Rate (m^3/d)				3335	11845	11845	11845	11845

Aquifer properties such as hydraulic conductivity, specific yield, specific storage, and porosity are mostly reasonable values, based on a review of literature on typical ranges of these properties. table 3 below shows reasonable values for these parameters. Some of the parameters in the model are outside of the ranges below, such as the specific storage values and the sandy loam hydraulic conductivity. However, these values were accepted anyway as they are within an order of magnitude of the bounds suggested by the cited sources, and are the result of model calibration. It is worth sacrificing some accuracy in the exact values of these parameters if it means the calibration procedure functioned correctly and the flow is following the expected path based on the physical properties of the aquifer. Note that the upper and lower bounds shown in table 3 below were not the same as the upper and lower bounds used during the calibration of the model (the bounds used during calibration were wider as to prevent parameter values calibrating to the upper or lower bound).

Table 3. Typical ranges of aquifer properties

Parameter	Lower Bound	Upper Bound	Source
Specific Yield, Medium Sand	0.15	0.32	(Johnson (USGS), 1976)
Specific Storage, Medium Sand	0.0000203	0.000492	(Wolff, 1982)
Horizontal and Vertical Hydraulic Conductivity, Medium Sand	0.078	43.2	(Duffield, 2019)
Specific Yield, Sandy Loam	0.25	0.67	(Johnson (USGS), 1976)
Specific Storage, Sandy Loam	0.000001	0.00004	(Wolff, 1982)
Horizontal and Vertical Hydraulic Conductivity, Medium Sand	0.5	2.2	(Rawls, 1998)
Porosity (Sand	0.05	0.5	(Yu, 1993)

The temporal discretization of the model is shown in table 4 below. The start and end dates for each stress period were carefully chosen to produce an accurate and efficient model. First, there is a steady state period prior to May 1, 2009 (day 0 in the simulation). This is stress period 1. On May 1, 2009, wells 2-8 began pumping. This change in pumping required the start of a new stress period (stress period 2), which lasts until June 1, 2017, which is when the MTBE release occurred, which changes the model and requires its own stress period. The time period from June 1, 2017 (day 2,953) through June 1, 2018 (day 3,318) is the time period in which MTBE is being released. The next time period is June 1, 2018 through June 1, 2024 (day 5,510) which represents the time period in which MTBE is moving through the aquifer but has stopped being released. Finally, the last stress period, stress period 5, is the stress period in which future pumping will take place, ranging from June 1, 2024 to December 31, 2039 (day 11,201 in the simulation). This stress period will have its own unique pumping rate, which means it must be separated from stress period 4. Large initial time steps are selected for steady periods in which the pumping rate does not change (time periods 3 and 4).

Table 4. Temporal discretization of model

Note that steps in time period 5 were changed for different simulations

Start Date	End Date	Stress Period	Model Starting Time	Model Ending Time	Length (Days)	Max. First Time Step (Days)	Multiplier	Steady State/ Transient	Drawdown Reference	Number of Steps (Calculated)
4/28/2009	4/30/2009	1	-1	0	1	1	1	Steady State	Yes	1
5/1/2009	6/1/2017	2	0	2953	2953	1	1.4	Transient	No	22
6/1/2017	6/1/2018	3	2953	3318	365	365	1.4	Transient	No	1
6/1/2018	6/1/2024	4	3318	5510	2192	500	1.4	Transient	No	4
6/1/2024	12/31/2039	5	5510	11201	5691	5691	1.4	Transient	No	1

The boundary heads and initial condition for the flow model are defined in order to produce an accurate model. The process of generating the boundary heads and implementing boundary conditions for the model is described in this section. First a new dataset is created in the project

file on ModelMuse-- which already has defined well data, domain, and discretization—and the measured heads found in table 3 in Appendix A are imported. Triangle interpolation is used for the boundary conditions in this model. To obtain head values at the start of the transient simulation, a steady state simulation is run in which wells 1 and 11 are pumping at rates of 3,120 m^3/day and 215 m^3/day, respectively. The resulting heads are the heads at the start of the transient simulation. The boundary heads are the heads along the domain boundary shown in the figure below.

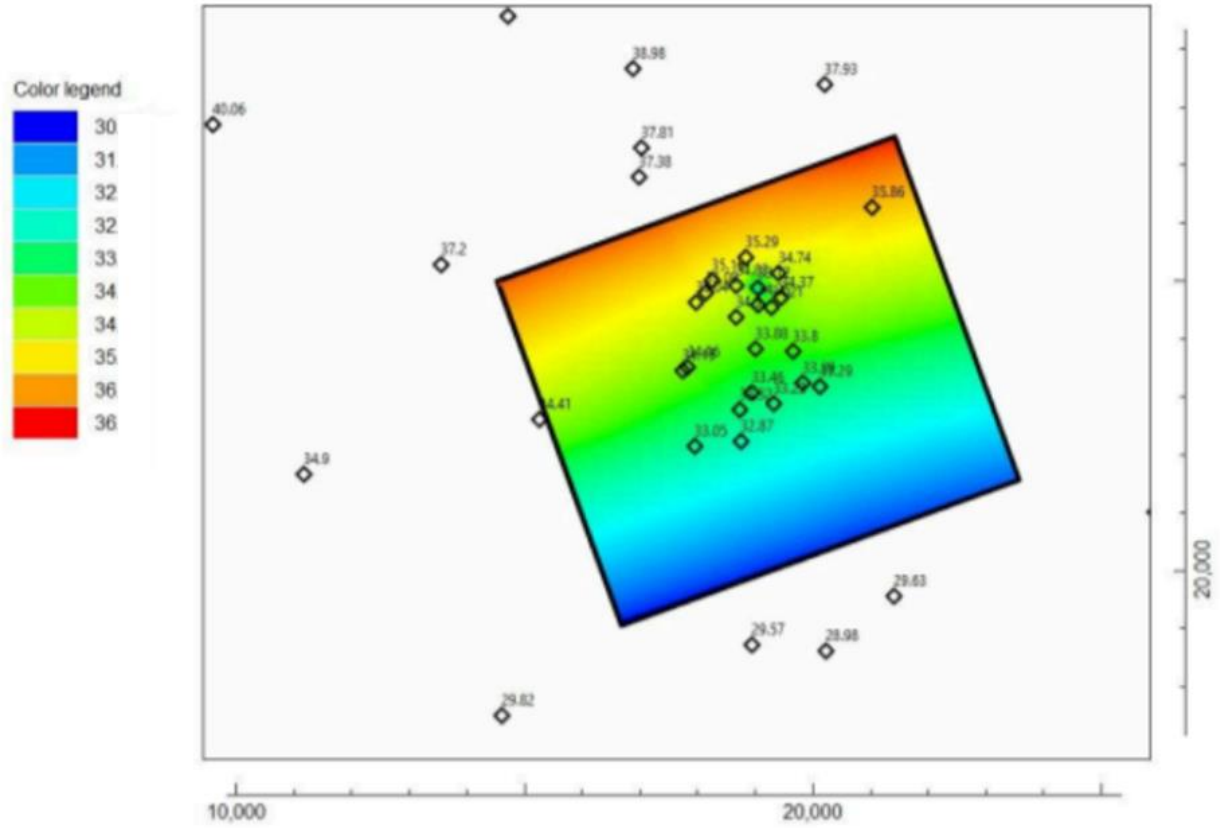

Figure 9a. CHD starting heads displayed as a color grid (Layer 1). The horizontal axis is the x coordinate in meters, the vertical axis is the y coordinate in meters. The head values displayed beside the well locations are the 2009 head values in meters. The color legend is in units of meters.

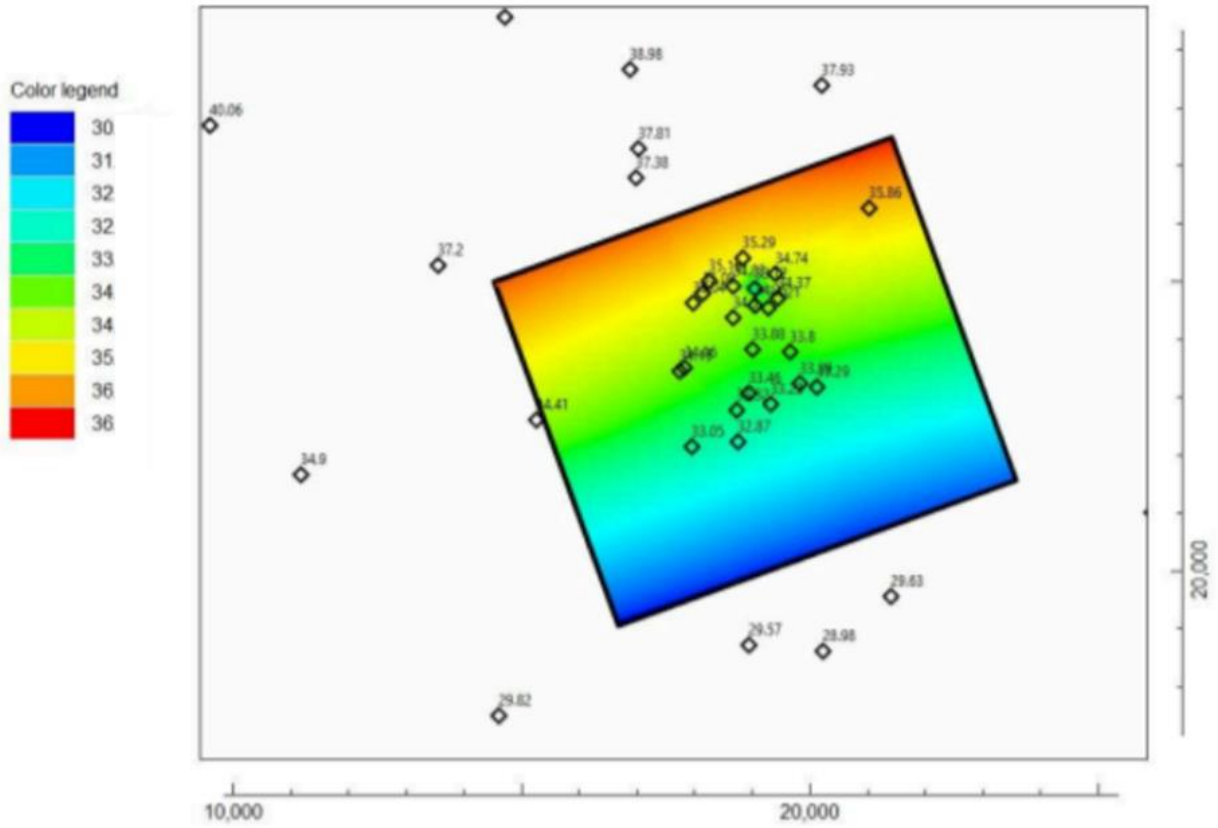

Figure 9b. CHD starting heads displayed as a color grid (Layer 2). The horizontal axis is the x coordinate in meters, the vertical axis is the y coordinate in meters. The head values displayed beside the well locations are the 2009 head values in meters. The color legend is in units of meters.

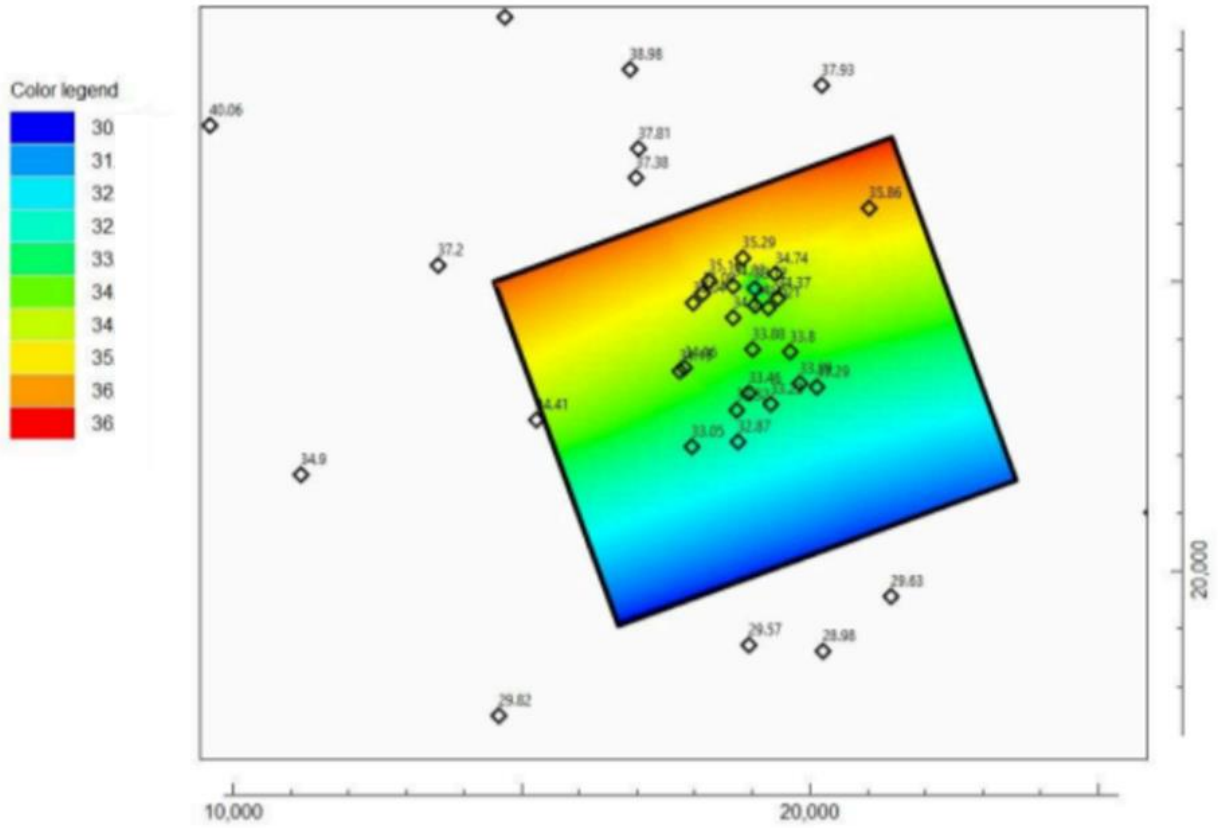

Figure 9c. CHD starting heads displayed as a color grid (Layer 3). The horizontal axis is the x coordinate in meters, the vertical axis is the y coordinate in meters. The head values displayed beside the well locations are the 2009 head values in meters. The color legend is in units of meters.

The Peclet number is an indication of the rate of advection relative to the rate of diffusion. It is important to analyze the Peclet number to determine the potential for numerical dispersion of the model with the parameters selected in the above section. The Peclet number is calculated as

$$P_e = \frac{\Delta x}{\alpha_L} = \frac{100\ m}{52.5\ m} = 1.90 \tag{16}$$

where Δx is the horizontal discretization in the primary direction of flow. The horizontal discretization varies spatially in the model, but most grid cells have $\Delta x = 100\ m$. This is an unconservative estimate of the Peclet number, however, because some grid cells have a smaller value of $\Delta x = 100\ m$. This Peclet number is acceptable as $P_e \leq 2$ reflects relatively low numerical dispersion.

Calibration Results: Flow Model

The parameters whose values are calibrated in the model are shown in the table below:

Table 5. Calibrated parameters

Calibrated Parameters
$K_{x,\ sand}$
$S_{y,\ sand}$
$S_{s,\ sand}$
$K_{x,\ Loam}$
$S_{y,\ Loam}$
$S_{s,\ Loam}$

The calibration and verification datasets are selected carefully to maximize the likelihood of success in calibration. Monitoring wells 1 through 4, 7 through 12, and 17-28 are outside of the model domain and therefore not used in the calibration or verification datasets.

Table 6. Calibration and verification datasets

Calibration Wells	Verification Wells
MW5	PW5
PW14	PW4
PW6	MW16
PW1	PW2
PW12	MW15
MW13	PW11
PW13	MW14
PW8	PW10
PW16	PW9
MW6	PW15
PW3	PW7
PW17	

The target calibration measures are based on the head variance across the domain and the anticipated accuracy of the model. The maximum magnitude residual is taken as one tenth of the maximum head variance across the domain (based on observed heads in tables 1A and 4A in Appendix A Typically, a smaller maximum magnitude of residuals is desired, but in this case because many assumptions were made in creating the model, for example the location of the sandy loam, a generous target is assigned for maximum magnitude of residuals.

The mean residual is expected to be significantly less than the maximum residual value, as in most datapoints the residual is expected to be quite small in order to ensure a somewhat accurate model. In this case, it is taken as one hundredth of the maximum head variance across the domain squared. The target for the sum of squared residuals is simply the mean residual multiplied by the number of observations.

Number of calibration observations: 72

Maximum head in domain: 36.84 meters

Minimum head in domain: 18.18 meters (well 7 in 2023)

Sum of squared residuals = $(\#\ of\ observations)(\frac{Head\ Drop}{100})^2 = (72)(\frac{36.84\ m - 18.18\ m}{100})^2 = 2.51\ m^2$

Maximum Magnitude of Residuals = $\frac{Head\ drop}{10} = \frac{36.84\ m - 18.18\ m}{10} = 1.87\ m$

Mean Residual = $(\frac{Head\ drop}{100})^2 = (\frac{36.84\ m - 18.18\ m}{100})^2 = 0.0348\ m$

Calibration was performed to estimate the values of six parameters. The hydraulic conductivity of the sand and sandy loam, the specific storage of the sand and sandy loam, and the specific yield of the sand and the sandy loam. The simulation was treated as transient for calibration. PEST was used to calibrate these parameters and PEST was run with 50 iterations.

The head observation data was divided into a calibration and verification dataset (see table 6) with data distributed in time and space. The target values for the calibration measures were then determined (see above). Next, the calibration was performed using PEST. First, the non-storage parameters were calibrated for just the steady state period and their values were set for the full calibration step. Using starting guesses for the parameters, and upper and lower bounds from prior research, all parameters were calibrated using PEST in the transient model. In this case, most of the parameters were not calibrated to upper or lower bounds, meaning the bounds were reasonable.

After calibrating the parameters with PEST, MATLAB was used to evaluate the calibration measures and compare them to the target calibration measures. The calibration dataset did not meet the target calibration measures, but the calibrated values were still considered accurate enough for the simulation. The verification dataset did not meet the calibration measure targets.

Table 7. Calibrated parameter values and sensitivities

Calibrated Parameter	Final Calibrated Value	Composite Scaled Sensitivity
$K_{x,\ sand}$	23.45 m/d	0.005 m
$S_{y,\ sand}$	0.525	0.02 m
$S_{s,\ sand}$	0.0000131 m^{-1}	1 m
$K_{x,\ Loam}$	2.31 m/d	0.04 m
$S_{y,\ Loam}$	0.150	0.01 m
$S_{s,\ Loam}$	0.00000999 m^{-1}	0.6 m

The specific yield of the sandy loam ($S_{y,\ Loam}$) was fixed. This is because the calibrated measure of sandy loam "bottomed out" which means it is the same as the lower bound of acceptable values. If calibration is run again with a smaller value of the lower bound, $S_{y,\ Loam}$ is likely to be less than 0.150, but this might represent compensation for an inaccuracy in the model, rather than a realistic value of $S_{y,\ Loam}$, so its value was fixed at the lower bound. All other parameters were calibrated. $K_{x,\ Loam}$ was manually calibrated, as the PEST calibration procedure resulted in a $K_{x,\ Loam}$ which caused physical impossibilities in the model (negative head values at wells).

The sensitivities of the calibrated parameters are not what is expected. Typically, the model is most sensitive to changes in hydraulic conductivity. The analysis was continued regardless.

Table 8. Measured Head, Simulated Head, and Residual. The notation "pw1_1" corresponds to an observation made at pumping well 1 on 4/30/2009, "_2" corresponds to the date 2/25/2010, "_3" corresponds to the date 1/9/2015, "_4" corresponds to the date 6/2/2018, "_5" corresponds to the date 4/16/2019, and "_6" corresponds to the date 12/23/2023. "pw" is pumping well and "mw" is monitoring well.

Observation	Measured	Calculated	Residual
	Value (m)	Value (m)	(m)
pw1_1	33.12	33.1182	1.79E-03
pw1_2	31.82	31.795	2.50E-02
pw1_3	30.83	30.7541	7.59E-02
pw1_4	30.58	30.641	-6.10E-02
pw1_5	30.53	30.6245	-9.45E-02
pw1_6	30.32	30.5866	-0.266596
pw2_1	34.25	33.8188	0.431229
pw2_2	31.56	31.6467	-8.67E-02
pw2_3	30.55	30.5288	2.12E-02
pw2_4	30.3	30.4038	-0.103799
pw2_5	30.25	30.3855	-0.135478
pw2_6	30.03	30.3431	-0.313082
pw3_1	34.5	34.2612	0.238813
pw3_2	22.23	27.6351	-5.40514
pw3_3	20.78	26.3797	-5.59968
pw3_4	20.34	26.2424	-5.90238
pw3_5	20.23	26.2222	-5.99222
pw3_6	19.89	26.1753	-6.28528
pw4_1	34.83	34.5166	0.313435
pw4_2	32.86	32.7485	0.111531
pw4_3	31.89	31.7799	0.110127
pw4_4	31.64	31.679	-3.90E-02
pw4_5	31.59	31.6644	-7.44E-02
pw4_6	31.39	31.6309	-0.240879
pw5_1	35.08	34.9567	0.123297
pw5_2	33.78	33.9257	-0.145684
pw5_3	32.86	33.0987	-0.238688
pw5_4	32.62	33.0074	-0.387434
pw5_5	32.57	32.9941	-0.424109
pw5_6	32.37	32.9633	-0.593265
pw6_1	35.29	35.0353	0.254651
pw6_2	34.3	34.1685	0.131469
pw6_3	33.41	33.421	-1.10E-02
pw6_4	33.17	33.3439	-0.173945
pw6_5	33.12	33.3329	-0.212889
pw6_6	32.93	33.3077	-0.377678
pw7_1	34	33.727	0.273015
pw7_2	20.85	27.7648	-6.9148
pw7_3	18.87	26.5163	-7.64625
pw7_4	18.53	26.3497	-7.81967

pw7_5	18.46	26.3242	-7.86424
pw7_6	18.18	26.2635	-8.08347
pw8_1	33.32	33.0819	0.238109
pw8_2	33	32.9212	7.88E-02
pw8_3	32.34	32.434	-9.40E-02
pw8_4	32.12	32.314	-0.194032
pw8_5	32.07	32.2944	-0.224364
pw8_6	31.88	32.2454	-0.365352
pw10_1	33.23	32.9507	0.279287
pw10_2	33	32.8349	0.16513
pw10_3	32.33	32.2819	4.81E-02
pw10_4	32.11	32.1544	-4.44E-02
pw10_5	32.07	32.1337	-6.37E-02
pw10_6	31.88	32.0824	-0.202444
pw11_1	34.06	34.0607	-7.07E-04
pw11_2	33.78	33.9166	-0.136649
pw11_3	33.03	33.3202	-0.29017
pw11_4	32.8	33.2122	-0.412243
pw11_5	32.75	33.1954	-0.445367
pw11_6	32.56	33.1545	-0.59447
pw12_1	34.21	33.8734	0.336607
pw12_2	33.36	32.7472	0.612799
pw12_3	32.47	31.6819	0.788089
pw12_4	32.23	31.555	0.674989
pw12_5	32.18	31.5363	0.643735
pw12_6	31.98	31.4927	0.487291
pw13_1	33.05	32.9547	9.53E-02
pw13_2	32.96	32.9326	2.74E-02
pw13_3	32.45	32.6325	-0.182541
pw13_4	32.26	32.5413	-0.281293
pw13_5	32.22	32.526	-0.306041
pw13_6	32.04	32.4875	-0.447502
pw14_1	35.16	35.0528	0.107177
pw14_2	34.17	34.2044	-3.44E-02
pw14_3	33.24	33.4059	-0.165905
pw14_4	33.01	33.3219	-0.311914
pw14_5	32.96	33.3097	-0.349749
pw14_6	32.76	33.2818	-0.521761
pw15_1	33.8	33.5516	0.248405
pw15_2	33.39	33.1611	0.228909
pw15_3	32.61	32.3033	0.306669
pw15_4	32.38	32.1654	0.214558
pw15_5	32.33	32.1442	0.185847
pw15_6	32.14	32.0932	4.68E-02

pw16_1	33.39	33.1544	0.235641
pw16_2	33.15	33.0037	0.146255
pw16_3	32.47	32.3601	0.109858
pw16_4	32.25	32.2292	2.08E-02
pw16_5	32.21	32.2083	1.67E-03
pw16_6	32.02	32.1575	-0.137486
pw9_1	33.29	33.082	0.208007
pw9_2	33.11	32.9898	0.12018
pw9_3	32.48	32.4263	5.37E-02
pw9_4	32.26	32.3029	-4.29E-02
pw9_5	32.22	32.2832	-6.32E-02
pw9_6	32.03	32.235	-0.204979
pw17_1	33.46	33.1357	0.324268
pw17_2	33.14	32.9448	0.195223
pw17_3	32.42	32.3546	6.54E-02
pw17_4	32.2	32.2253	-2.53E-02
pw17_5	32.15	32.2043	-5.43E-02
pw17_6	31.96	32.1526	-0.192552
mw5_1	35.04	34.955	8.50E-02
mw5_2	34.28	34.2991	-1.91E-02
mw5_3	33.39	33.518	-0.12804
mw5_4	33.16	33.4262	-0.266231
mw5_5	33.11	33.4127	-0.302715
mw5_6	32.91	33.3812	-0.471228
mw6_1	35.86	35.7917	6.83E-02
mw6_2	35.81	35.7805	2.95E-02
mw6_3	35.35	35.6381	-0.288127
mw6_4	35.16	35.6134	-0.453362
mw6_5	35.12	35.6097	-0.489748
mw6_6	34.95	35.6015	-0.651532
mw13_1	34.15	34.0736	7.64E-02
mw13_2	33.89	33.9523	-6.23E-02
mw13_3	33.16	33.386	-0.226006
mw13_4	32.93	33.2799	-0.349942
mw13_5	32.89	33.2633	-0.373301
mw13_6	32.7	33.2229	-0.522894
mw14_1	32.87	32.7223	0.147655
mw14_2	32.75	32.678	7.20E-02
mw14_3	32.19	32.3123	-0.122278
mw14_4	31.99	32.2063	-0.216274
mw14_5	31.94	32.1886	-0.248574
mw14_6	31.76	32.1439	-0.383946
mw16_1	34.74	34.5014	0.238577
mw16_2	34.05	33.9064	0.143617
mw16_3	33.17	33.0497	0.120251
mw16_4	32.94	32.9509	-1.09E-02
mw16_5	32.89	32.9366	-4.66E-02
mw16_6	32.69	32.9037	-0.213659
mw15_1	34.37	34.0402	0.329836
mw15_2	33.62	33.2416	0.3784
mw15_3	32.74	32.2528	0.487161
mw15_4	32.5	32.1334	0.366603
mw15_5	32.45	32.1158	0.334186
mw15_6	32.25	32.0751	0.174932

Calibration Measures and Discussion

The numerical calibration measures are shown in the tables below for both the calibration and verification datasets. Using the PEST calibrated value of $K_{x,loam} = 1.26\ m/d$ (which causes wells to run dry), the following calibration measures are produced:

Table 9. Calibration measures for original calibrated parameters (not used in final model)

	Calibration Dataset Calibration Measures	Target Calibration Measures
Sum of Squared Residual	6.95 m^2	2.51 m^2
Magnitude of Mean Residual	-0.0483 m	0.0348 m
Maximum Magnitude of Residual	0.821 m	1.87 m

	Verification Dataset Calibration Measures	Target Calibration Measures
Sum of Squared Residual	21.6 m^2	2.51 m^2
Magnitude of Mean Residual	-0.140 m	0.0348 m
Maximum Magnitude of Residual	0.510 m	1.87 m

When the $K_{x,loam}$ is manually calibrated, resulting in a value of 2.31 m/d, the calibration measures become extremely high (poor calibration).

Table 10. Calibration measures for parameters used in the final model (calibrated and fixed)

	Calibration Dataset Calibration Measures	Target Calibration Measures
Sum of Squared Residual	177 m^2	2.51 m^2
Magnitude of Mean Residual	-4.54 m	0.0348 m
Maximum Magnitude of Residual	6.29 m	1.87 m

	Verification Dataset Calibration Measures	Target Calibration Measures
Sum of Squared Residual	299 m^2	2.51 m^2
Magnitude of Mean Residual	-0.584 m	0.0348 m
Maximum Magnitude of Residual	8.08 m	1.87 m

Even though the calibration targets are extremely poor in the latter case, this model will take $K_{x,loam} = 2.31\ m/d$, because it results in the expected flow behavior. Ideally, the calibration measures would match the target calibration measures, but in this case, it is too difficult to match the calibration measures and maintain a logical flow in the aquifer. One significant reason for the poor calibration measures is the unknown location of the sandy loam region.

Spatial Bias

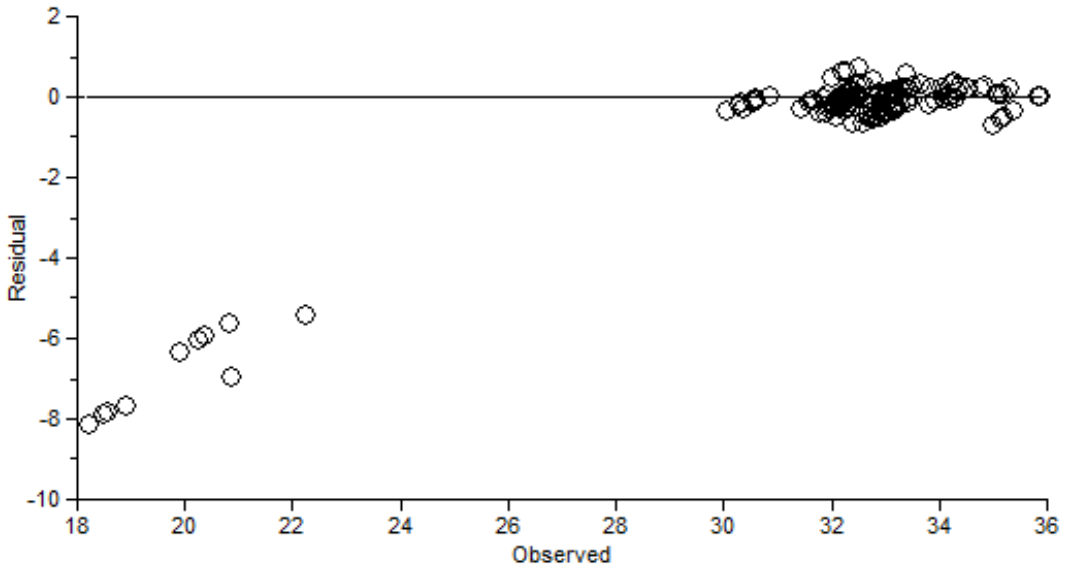

Figure 10. Plot of residual (meters) versus observed head (meters) from MODFLOW

This plot does not display spatial bias. The residuals are not dependent on the observed heads (which vary spatially). If there was spatial bias, some pattern of residual values varying with observed head would appear, but in the above graph there is no particular pattern in which residuals vary with observed head.

Plots of Observed and Simulated Head Versus Time

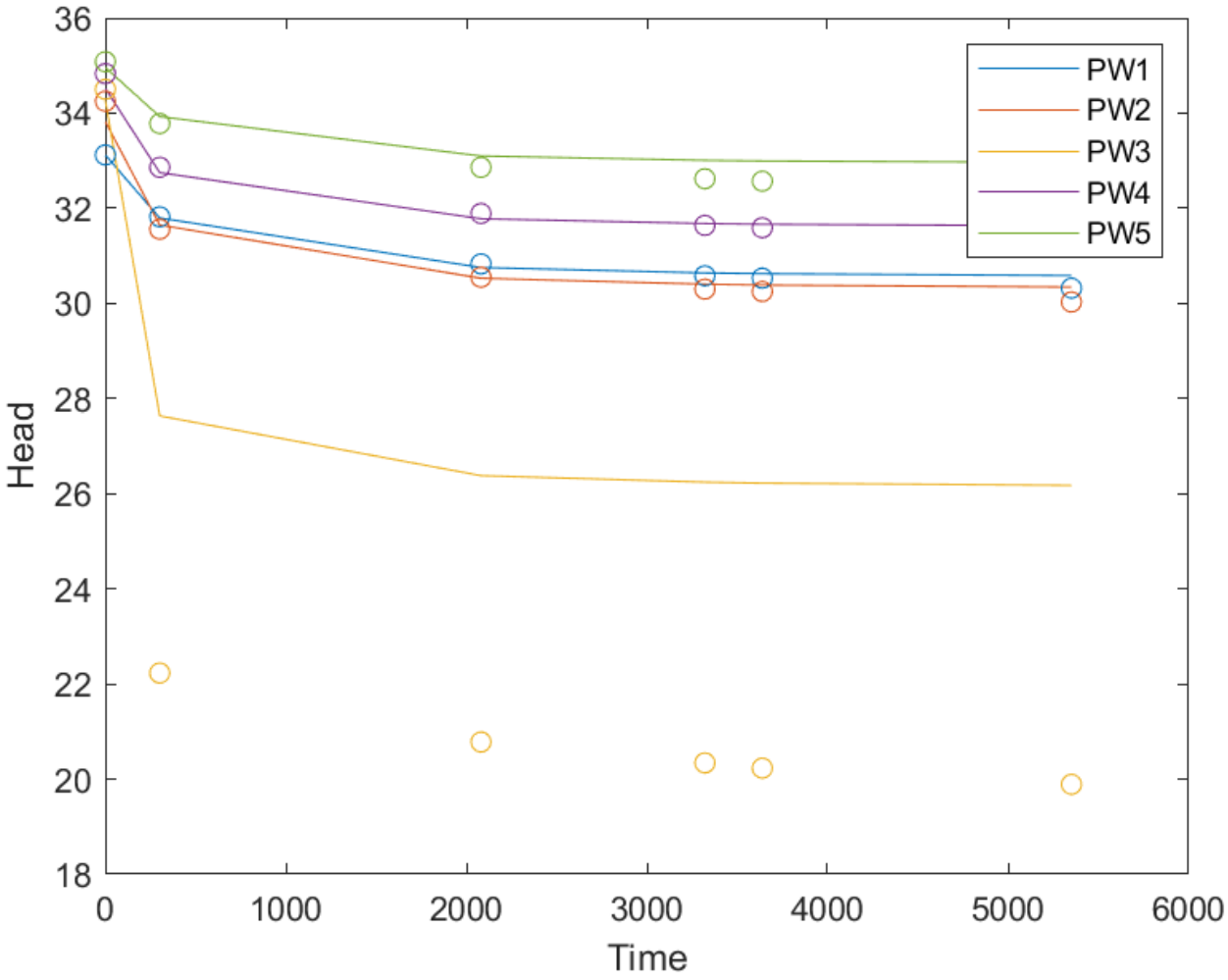

Figure 11. Head (m) versus time (days) for pumping and monitoring wells from MODFLOW

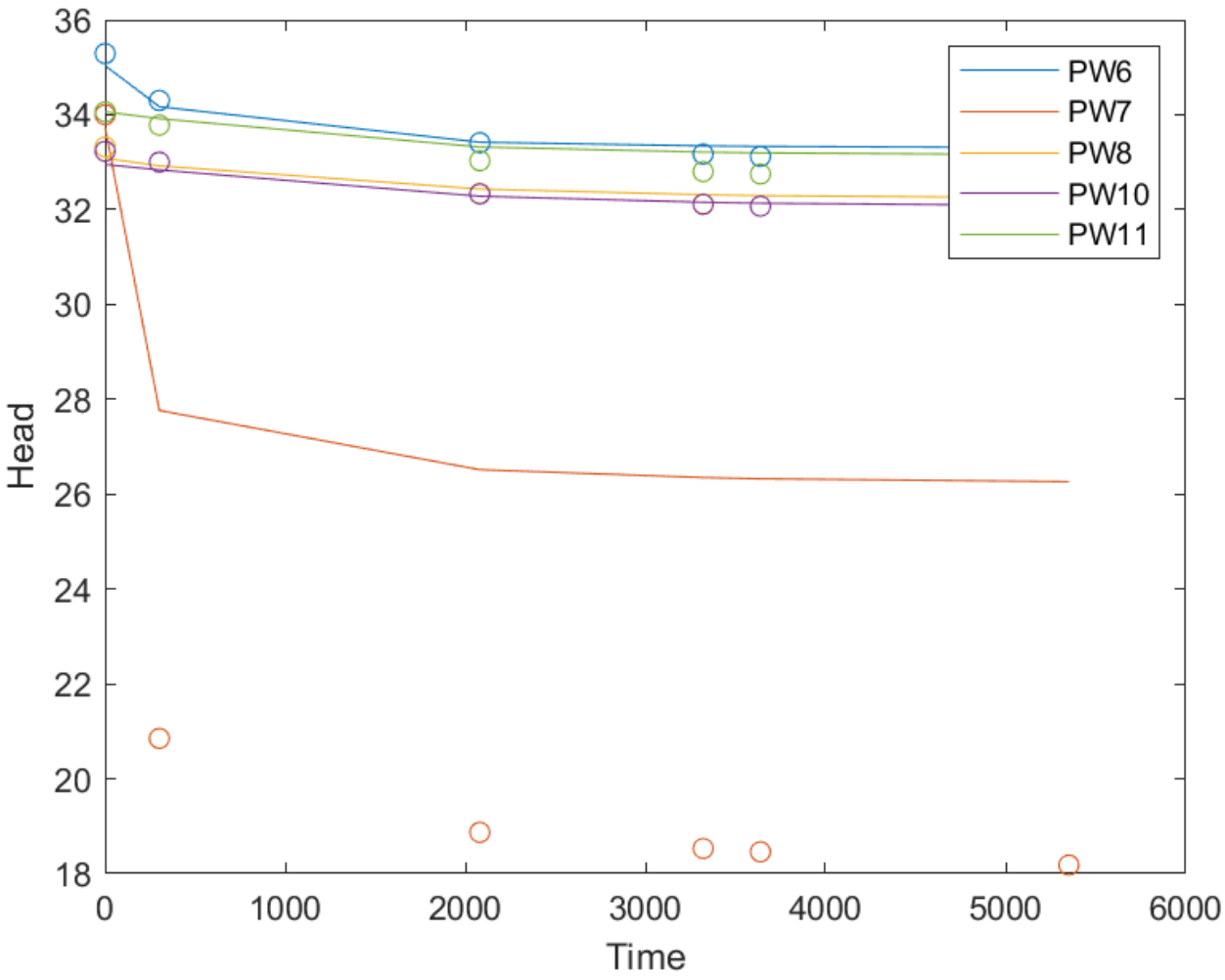

Figure 12. Head (m) versus time (days) for pumping and monitoring wells from MODFLOW

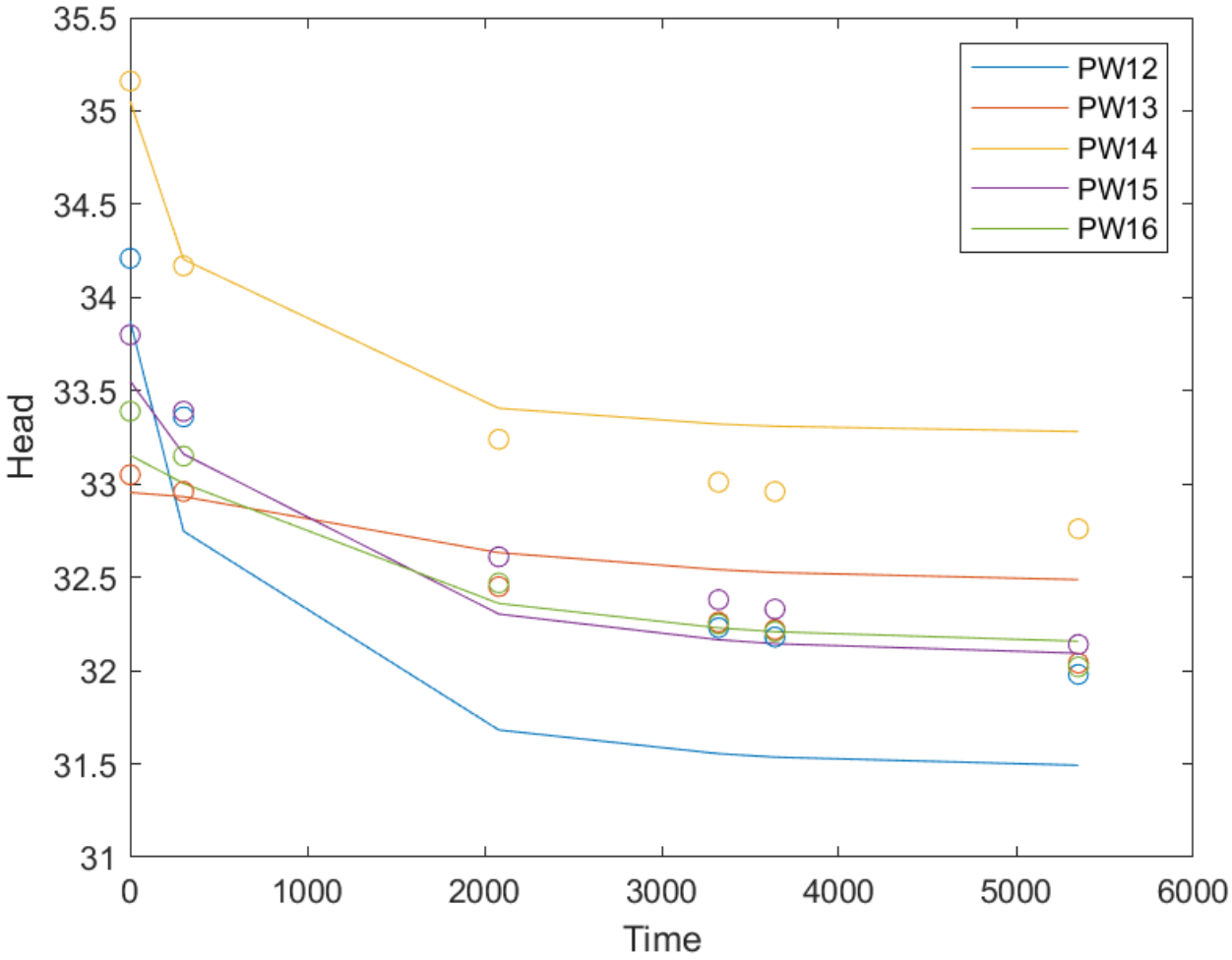

Figure 13. Head (m) versus time (days) for pumping and monitoring wells from MODFLOW

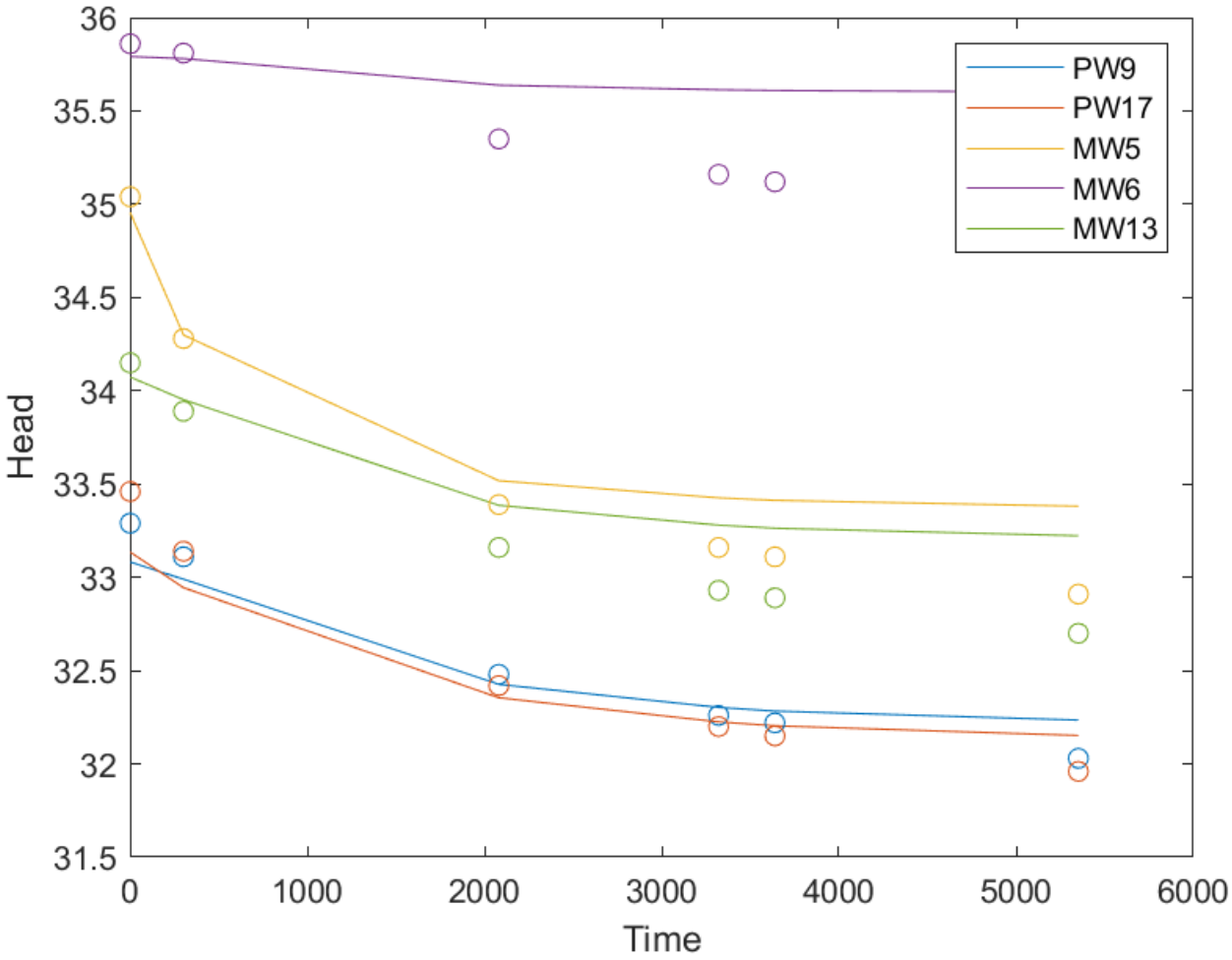

Figure 14. Head (m) versus time (days) for pumping and monitoring wells from MODFLOW

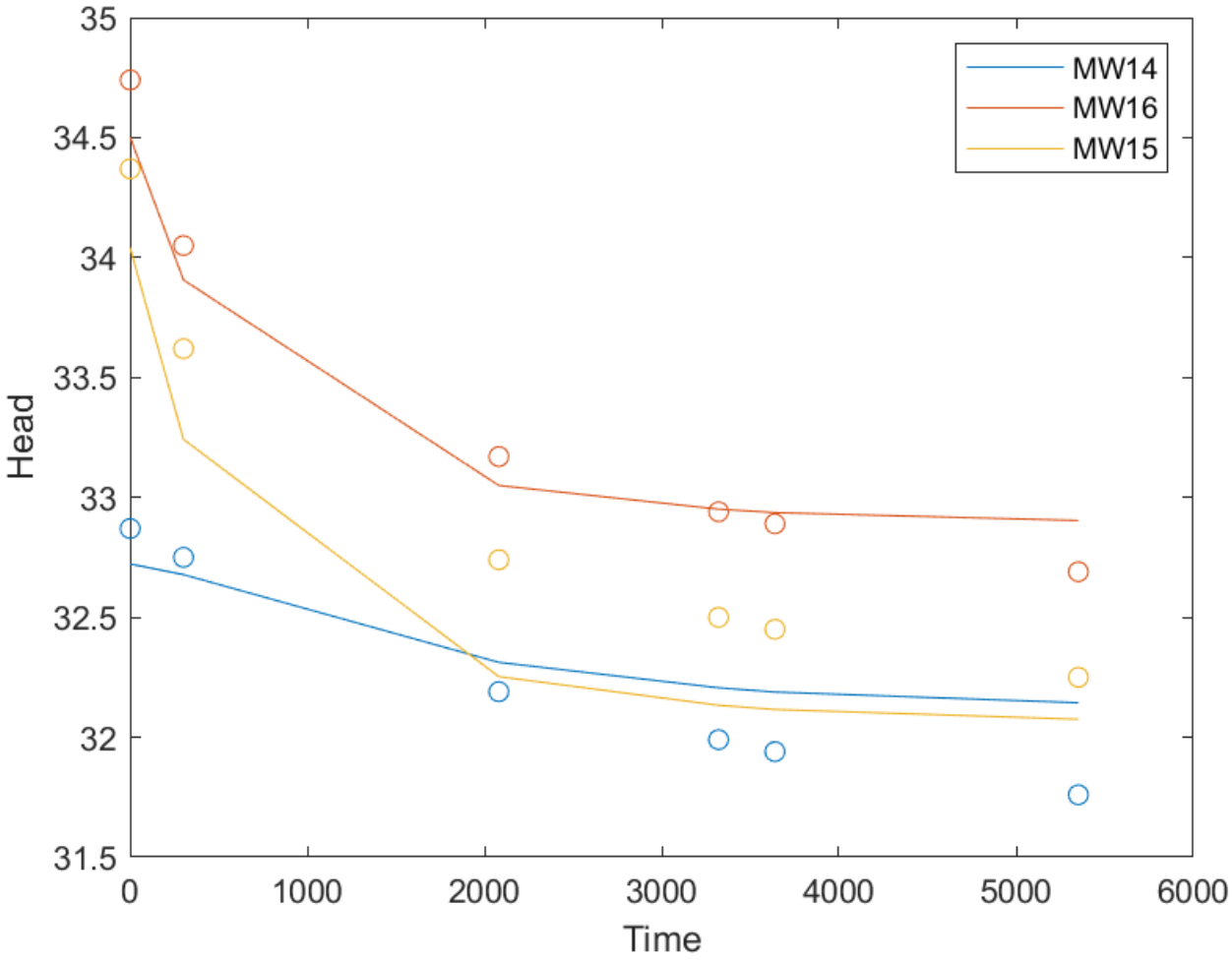

Figure 15. Head (m) versus time (days) for pumping and monitoring wells from MODFLOW

The head distribution in April 2009 and December 2023 is generated with the calibrated parameter values (shown in figures 16 and 17 below). These head distributions are appropriate as the direction of flow is as expected in the conceptual model and no wells are running dry.

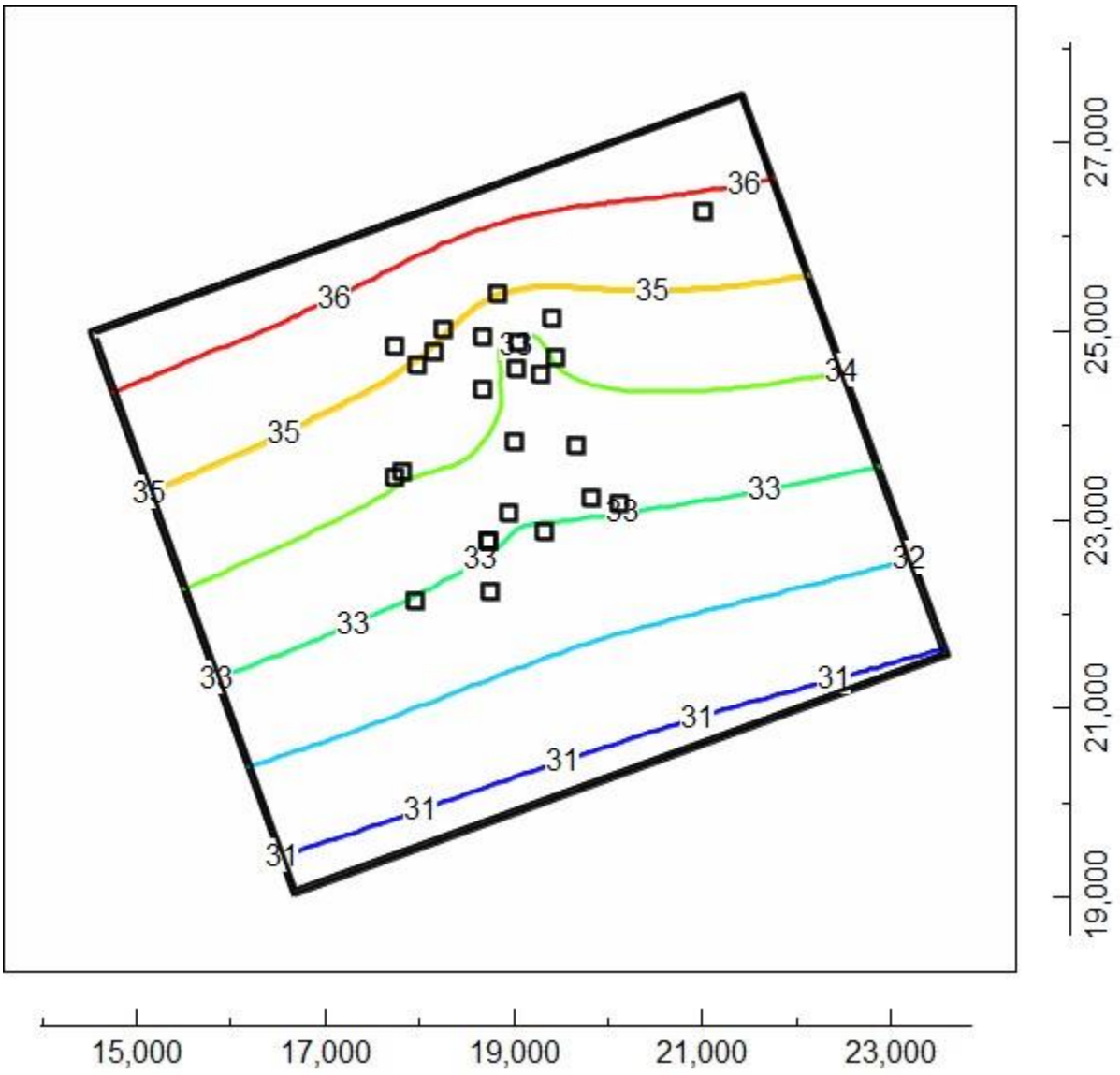

Figure 16. Head contours (m) distribution over aquifer domain in layer 01 in April 2009. The horizontal axis is the x spatial coordinate (m) and the vertical axis is the y spatial coordinate (m)

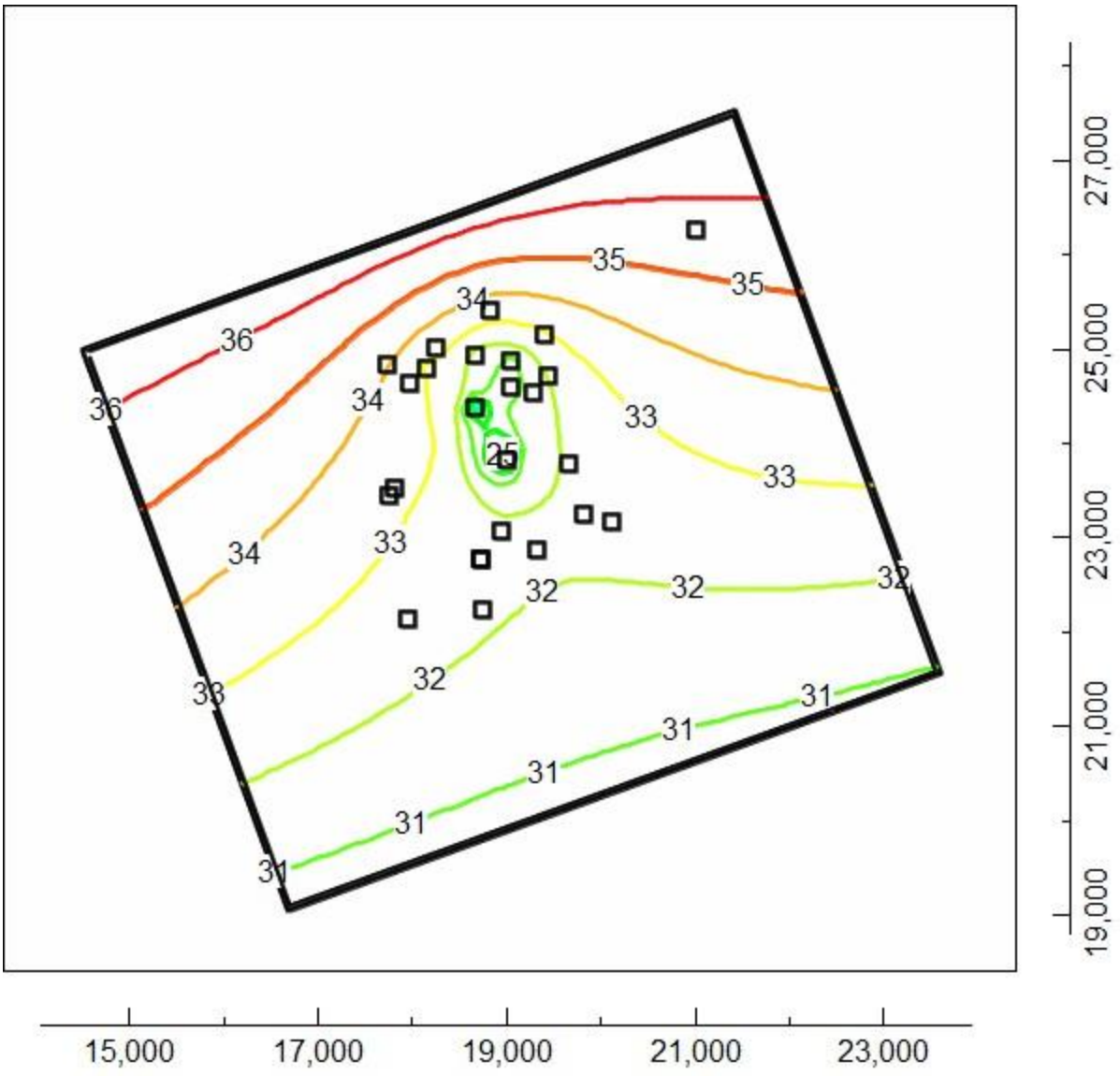

Figure 16. Head contours (m) distribution over aquifer domain in layer 01 in December 2023. The horizontal axis is the x spatial coordinate (m) and the vertical axis is the y spatial coordinate (m).

Calibration Results: Transport Model

Table 11. Transport calibrated parameters

Calibrated Parameters
Porosity
Longitudinal Dispersivity
Transverse Dispersivity

Calibration is based on the observations at pumping well 5 and monitoring well 5, as these wells are the only ones that have observations throughout the entire time period as well as an identifiable peak in the observation data. These wells also see the highest concentrations of MTBE. There is no verification dataset. Other well observation data was incomplete and thus most wells were not used for calibration (only PW5 and MW5 are used).

The time of peak concentration is affected simply by changing the porosity, while the maximum concentration is more difficult to match for MW5 and PW5 as it relies on a combination of factors, but primarily the longitudinal dispersivity. Therefore, when choosing calibration measures, it is expected that the time of peak concentration will be simpler to calibrate than the peak concentration itself. The selected calibration targets are shown below.

$$\Delta C_{max} \leq 0.2 C_{max}$$

$$\Delta T_{max} \leq 0.05 T_{max}$$

where ΔC_{max} is the difference between the measured and simulated maximum concentration (g/m^3), ΔT_{max} is the difference between the measured and simulated time of maximum concentration. Samples were taken every 3 months, which prevents an extremely low target on ΔT_{max}

The calibration procedure is significantly different than the procedure for flow parameter calibration, and requires manual calibration. Initial values of porosity, longitudinal dispersivity, and transverse dispersivity were entered into ModelMuse along with the observed concentration data. The simulation was run with MT3D- USGS and MATLAB was used to convert the results of the .mto files into plots of concentration versus time. The parameters were then calibrated manually. Porosity was adjusted to match the timing of the peak concentration and longitudinal dispersivity was changed to match the magnitude of peak concentration and spread of the breakthrough curve. All of these adjustments were made to the Modelmuse file and then a new .mto file was generated until most of the parameter measures met the target parameter measures. The calibrated parameter values are shown in the table below.

Table 12. Final values of calibrated parameter values

Parameters	Calibrated Parameter Values
Porosity	0.15
Longitudinal Dispersivity	52.5 m
Transverse Horizontal Dispersivity	5.25 m

Table 13. Target and actual values of the calibration measures

	C_{max} (g/m^3)	T_{max} (d)	▲C_{max} (g/m^3)	▲T_{max} (d)	Target ▲T_{max} (d)	Target ▲C_{max} (g/m^3)
Pumping Well 5	0.64	3699	0.0031	169	185	0.13
Monitoring Well 5	0.78	3808	0.25	152	190	0.16

The simulated results meet the calibration targets well temporally. Pumping well 5 also meets the calibration target for ΔC_{max}. The only calibration target not met is ΔC_{max} for monitoring well 5. Due to the nature of the model, it is too difficult to match both pumping well 5 and monitoring well 5 breakthrough curves and peak concentrations without changing the calibrated parameters of flow. The ΔC_{max} is within an order of magnitude of the target and it would make the model too inaccurate in other ways to modify extra parameters just to fit the transport parameters. These are not intended to be perfect, but are expected to somewhat fit the breakthrough curve. Overall, these values are acceptable as they generally meet the targets and the target not met is within an order of magnitude.

The reasons for the difference between the simulated breakthrough curves and the observations based on table 5A in Appendix A is the unknown location of the sandy loam. See figure 17 for the breakthrough curves. There are also inaccuracies and assumptions with the flow parameters, which can effect the transport model significantly. Ultimately, the transport parameters are not perfect, but are suitable for the model given the amount of unknown information and assumptions.

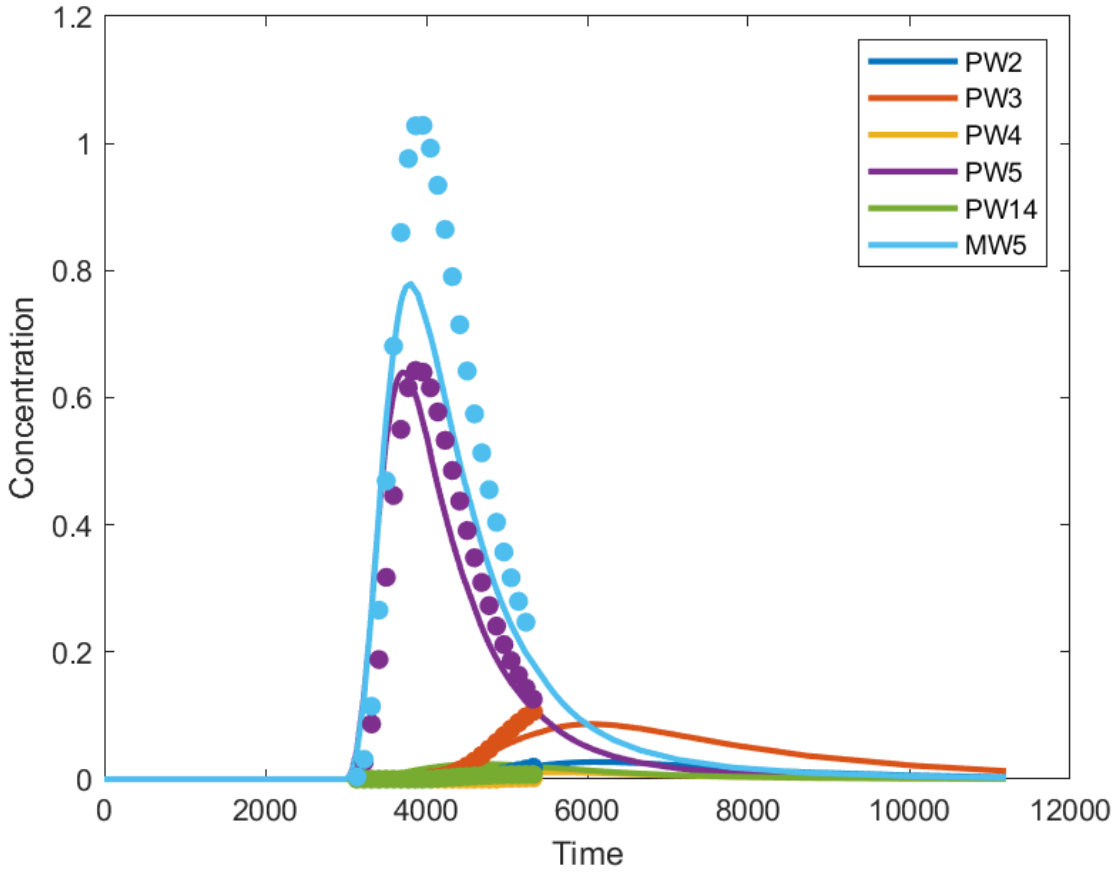

Figure 17. Simulated versus observed concentration breakthrough curves. Concentration is in the units of grams per meter cubed and time is in units of days. Simulated concentration is shown as a continuous line while observations are points.

Table 14. MATLAB output of simulated and observed maximum concentrations and concentration times.

	Simulated		Observed	
Well	C_{max} (g/m^3)	T_{max} (d)	C_{max} (g/m^3)	T_{max} (d)
PW5	0.64	3699	0.64	3868
MW5	0.78	3808	1.03	3959

Final Pumping Scheme June 2024 to December 2039

A final pumping scheme is selected for the time period from June 1, 2024 to December 21, 2039 which maintains a pumping rate of 11,845 m^3/day (consistent with the rate of time periods 2-4) while ensuring that the concentration of MTBE is less than 0.013 mg/L. The pumping scheme is shown in the table below:

Table 15. Pumping rates for each time period. Final pumping scheme is the column labeled "Pumping Rate Time Period 5"

Well ID	x Coordinate (m)	y Coordinate (m)	Head 2009 (m)	Pumping Rate, Time Period 1 (m^3/d)	Pumping Rate, Time Period 2 (m^3/d)	Pumping Rate, Time Period 3 (m^3/d)	Pumping Rate Time Period 4 (m^3/d)	Pumping Rate, Time Period 5 (m^3/d)
				April 30, 2009	May 1, 2009 - June 1, 2017	June 1, 2017 - June 1, 2018	June 1, 2018 - June 1, 2024	June 1, 2024 - December 31, 2039
PW1	19042	24881	33.12	3120	3120	3120	3120	0
PW2	19035	24597	34.25	0	2120	2120	2120	0
PW3	18672	24384	34.5	0	1460	1460	1460	0
PW4	18664	24932	34.83	0	1780	1780	1780	0
PW5	18145	24788	35.08	0	980	980	980	0
PW6	18825	25399	35.29	0	520	520	520	2000
PW7	19008	23829	34	0	1470	1470	1470	0
PW8	18733	22774	33.32	0	180	180	180	0
PW9	20109	23175	33.29	0	0	0	0	2000
PW10	19321	22876	33.23	0	0	0	0	0
PW11	17814	23513	34.06	215	215	215	215	250
PW12	19280	24543	34.21	0	0	0	0	0
PW13	17953	22136	33.05	0	0	0	0	3500
PW14	18249	25013	35.16	0	0	0	0	0
PW15	19660	23790	33.8	0	0	0	0	1845
PW16	19818	23241	33.39	0	0	0	0	2000
PW17	18943	23076	33.46	0	0	0	0	250
Total Pumping Rate (m^3/d)				3335	11845	11845	11845	11845

As seen in the table, the sum of the well pumping rates of time period 5 is 11,845 m^3/day. Additional evidence can be found in the .wel file output from the simulation.

Simulation Results With Final Pumping Scheme for June 2024 to December 2039

First, it is verified that changing the pumping scheme does not cause a reversal of flow at the boundaries, changing the flow conditions of the model. This is accomplished by generating contour plots of spatially varying head in the aquifer domain. These plots are shown below.

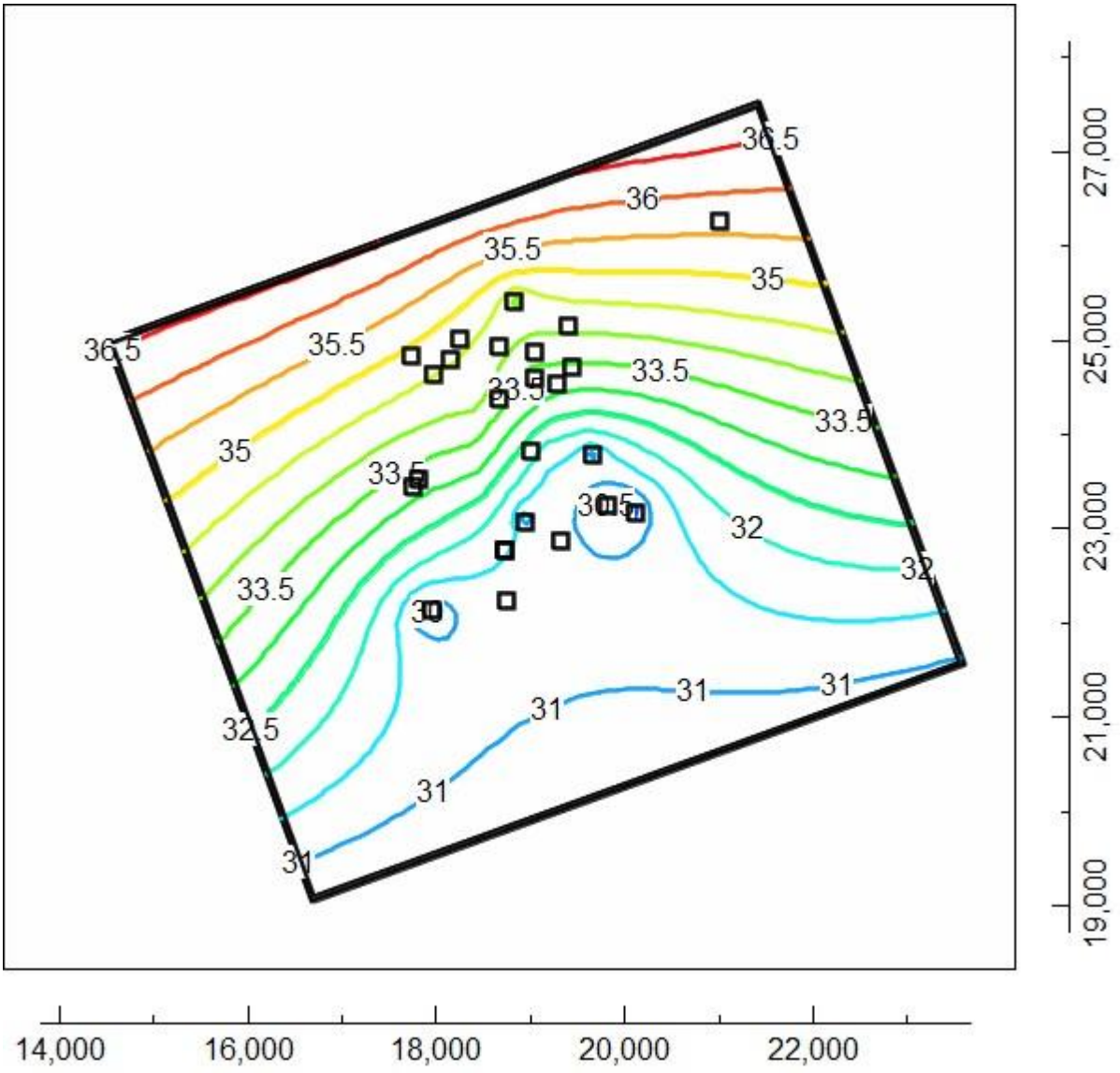

Figure 18. Plot of head (m) distribution over aquifer domain in layer 1 in December 2039. The horizontal axis is the x spatial coordinate (m) and the vertical axis is the y spatial coordinate (m)

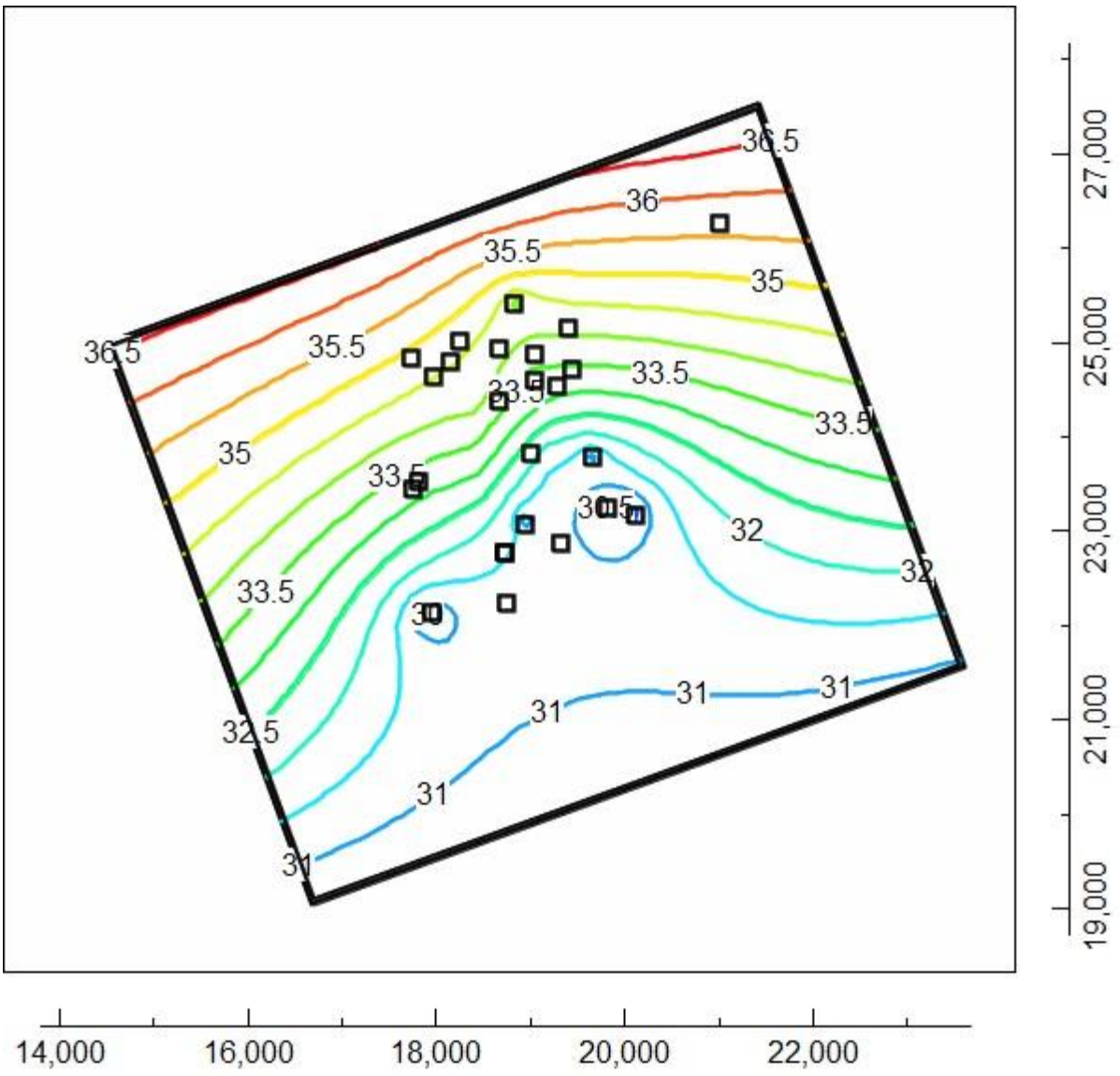

Figure 19. Plot of head (m) distribution over aquifer domain in layer 2 in December 2039. The horizontal axis is the x spatial coordinate (m) and the vertical axis is the y spatial coordinate (m)

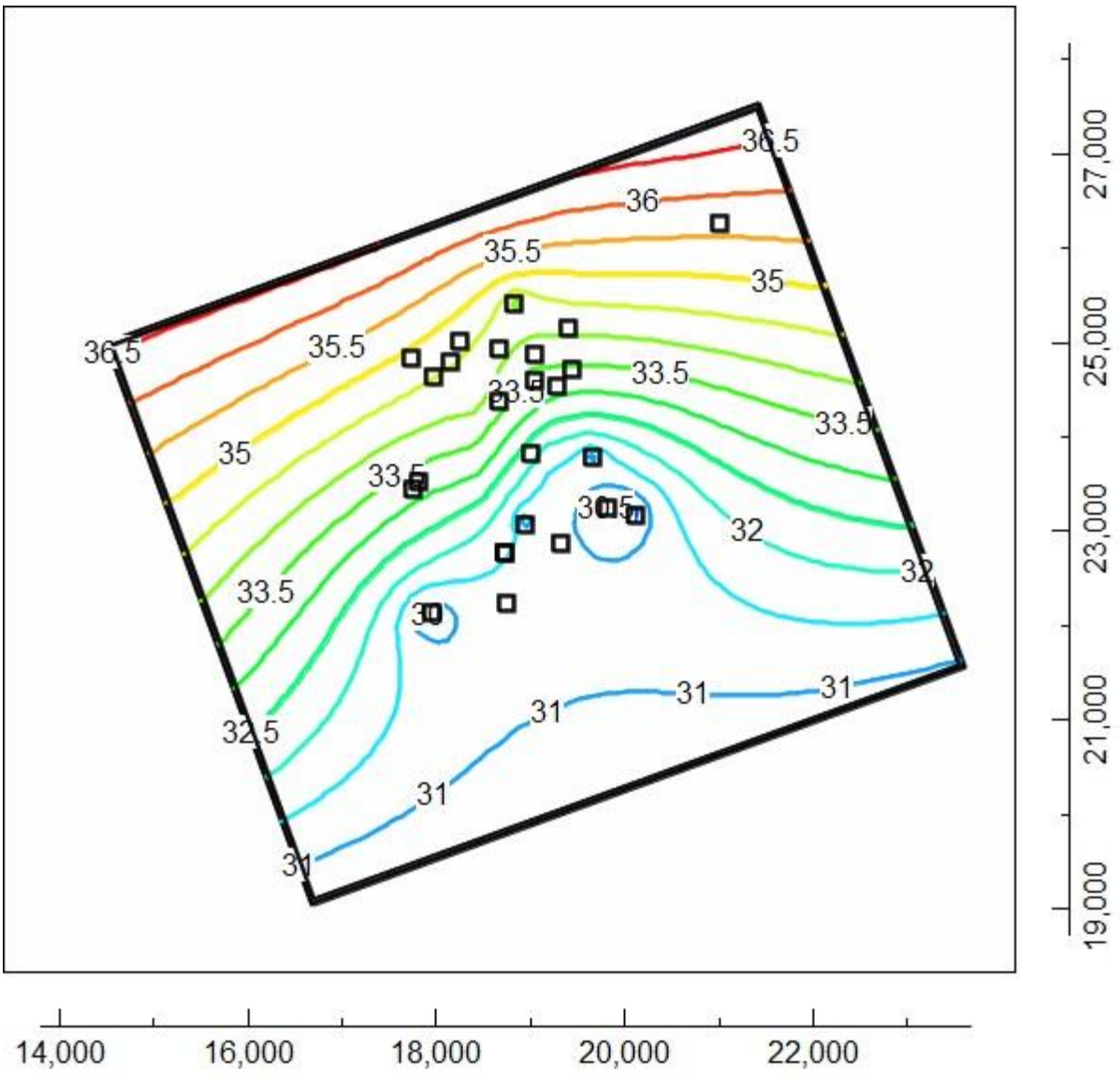

Figure 20. Plot of head (m) distribution over aquifer domain in layer 3 in December 2039. The horizontal axis is the x spatial coordinate (m) and the vertical axis is the y spatial coordinate (m)

Head decreases in the flow direction throughout the extent of the domain, showing that the new pumping scheme does not result in a reversal of flow at the boundaries.

Additionally, it is demonstrated by the figure below that the concentration of MTBE does not exceed the maximum 0.015 g/m^3. The wells are all drawing water from layer three, so only the concentration for layer 3 is shown.

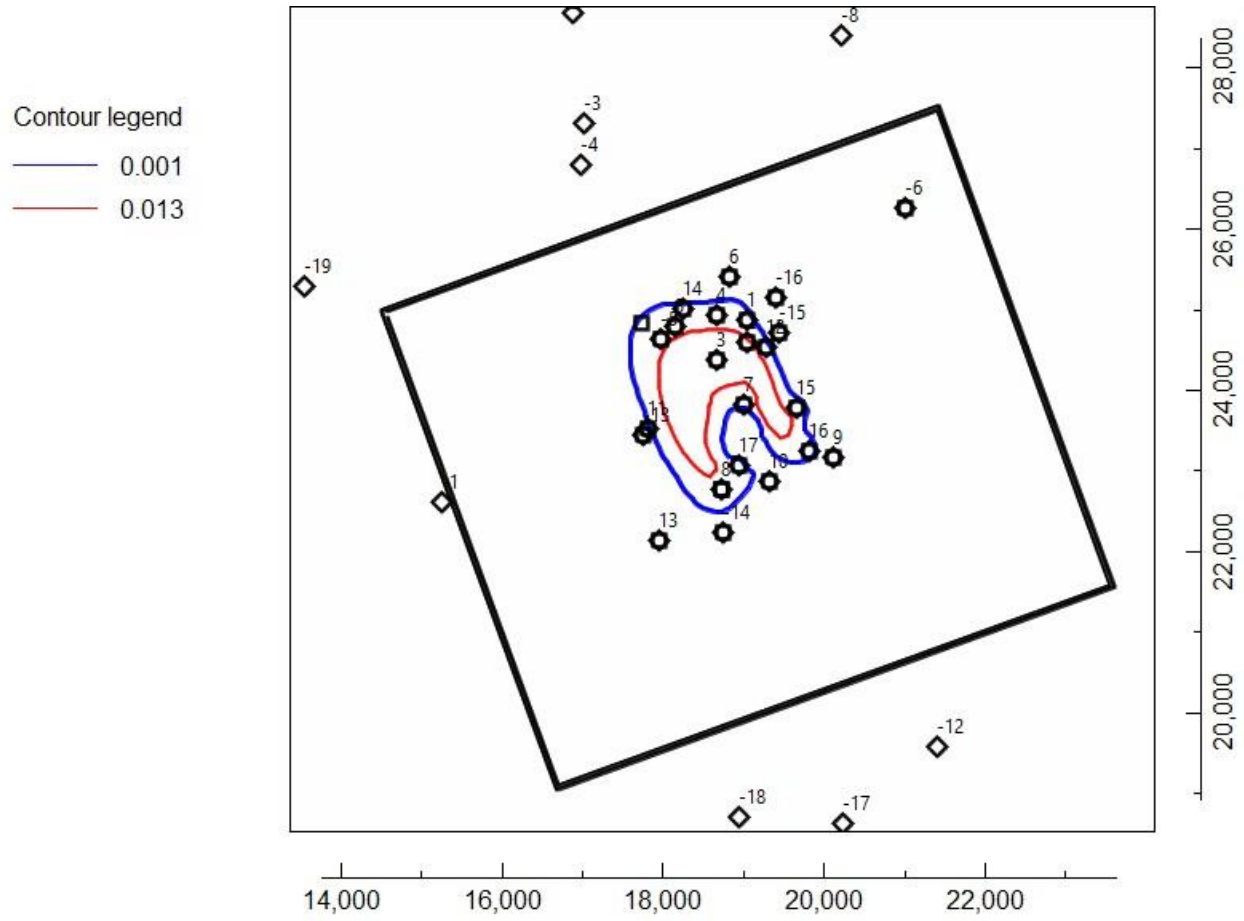

Figure 21. MTBE Plume in December 2039, layer 3. Concentration contours are in units of g/m^3. The horizontal axis is the x spatial coordinate (m) and the vertical axis is the y spatial coordinate (m). Monitoring wells are denoted with a "-" sign.

The breakthrough curve is plotted to demonstrate that the concentrations of MTBE in pumping wells for the final period (2024- 2039) are below the acceptable limit. Additional wells are included, as any wells which could be affected by the concentration plume are shown in the plot below. Only wells which are well outside the extent of the plume are omitted from the breakthrough curve (wells 13, 14, 18, and 9). Table 15 contains necessary information for which wells are pumping at any given time period.

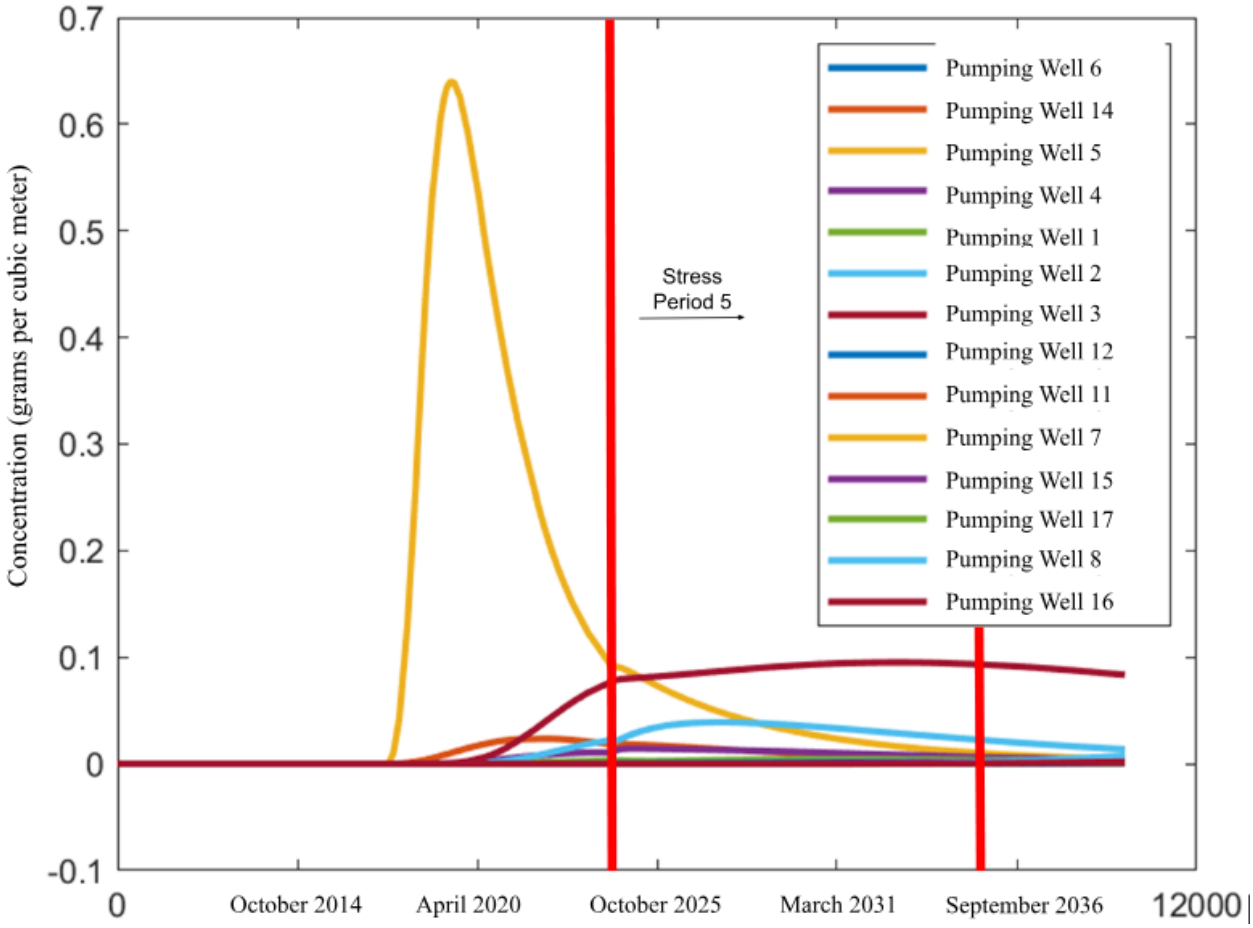

Figure 22. Breakthrough curve, showing only wells 5, 2, 3, 4, and 14 exceed the concentration for stress period 5. These wells are not pumping during this stress period.

Finally, the head versus time graph for all wells is shown below to prove that this pumping scheme does not cause any wells to run dry (negative heads at the well locations).

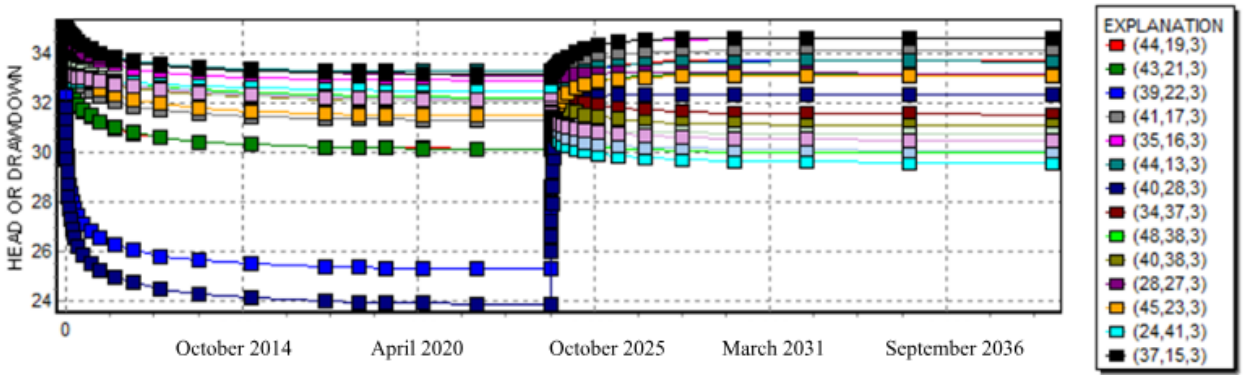

Figure 23 Head (m) (layer 3) versus date for all pumping wells.

Table 16. Pumping well rows and columns

Pumping Well	Row	Column
1	19	44
2	21	43
3	22	39
4	17	41
5	16	35
6	13	44
7	28	40
8	37	34
9	38	48
10	38	40
11	27	28
12	23	45
13	41	24
14	15	37
15	31	46
16	37	46
17	35	37

Part 8: Uncertainty Analysis – Monte Carlo Simulations

Five different realizations of hydraulic conductivity distribution were generated for the medium sand region of the aquifer. The mean hydraulic conductivity is set to the calibrated value of hydraulic conductivity of the medium sand layer and a standard deviation of ln(k) = .25 is selected, indicating a mildly heterogeneous aquifer. The different hydraulic conductivity fields are labelled A-E and are described below. The concentration plume, head versus time, and breakthrough curve are generated for each realization to prove the selected pumping scheme works with different realizations of the hydraulic conductivity field.

Hydraulic Conductivity Distribution A

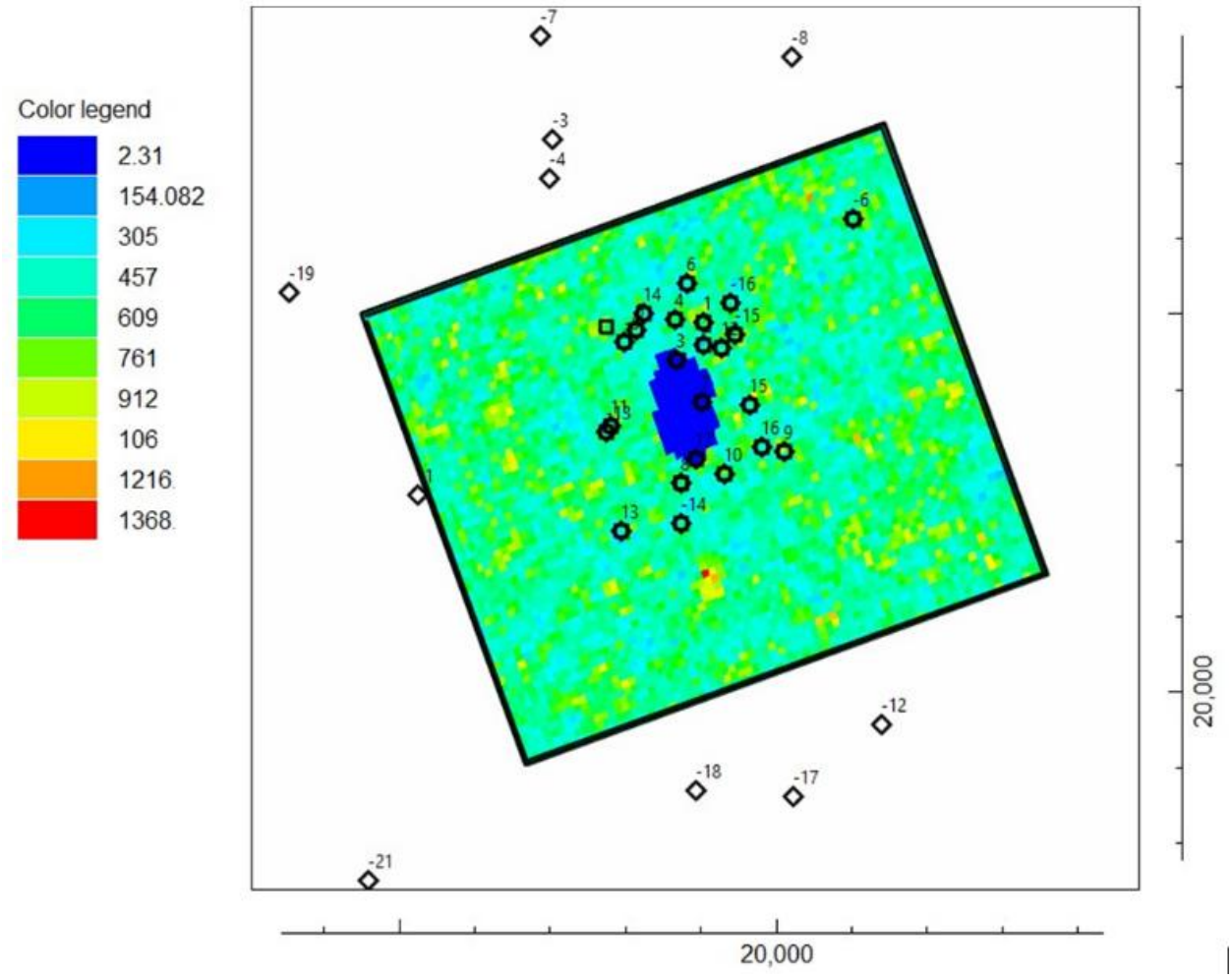

Figure 24. Hydraulic conductivity distribution A. The color legend indicates the hydraulic conductivity in the units of meters per day. The horizontal axis is the x spatial coordinate (m) and the vertical axis is the y spatial coordinate (m). Monitoring wells are denoted with a "-" sign.

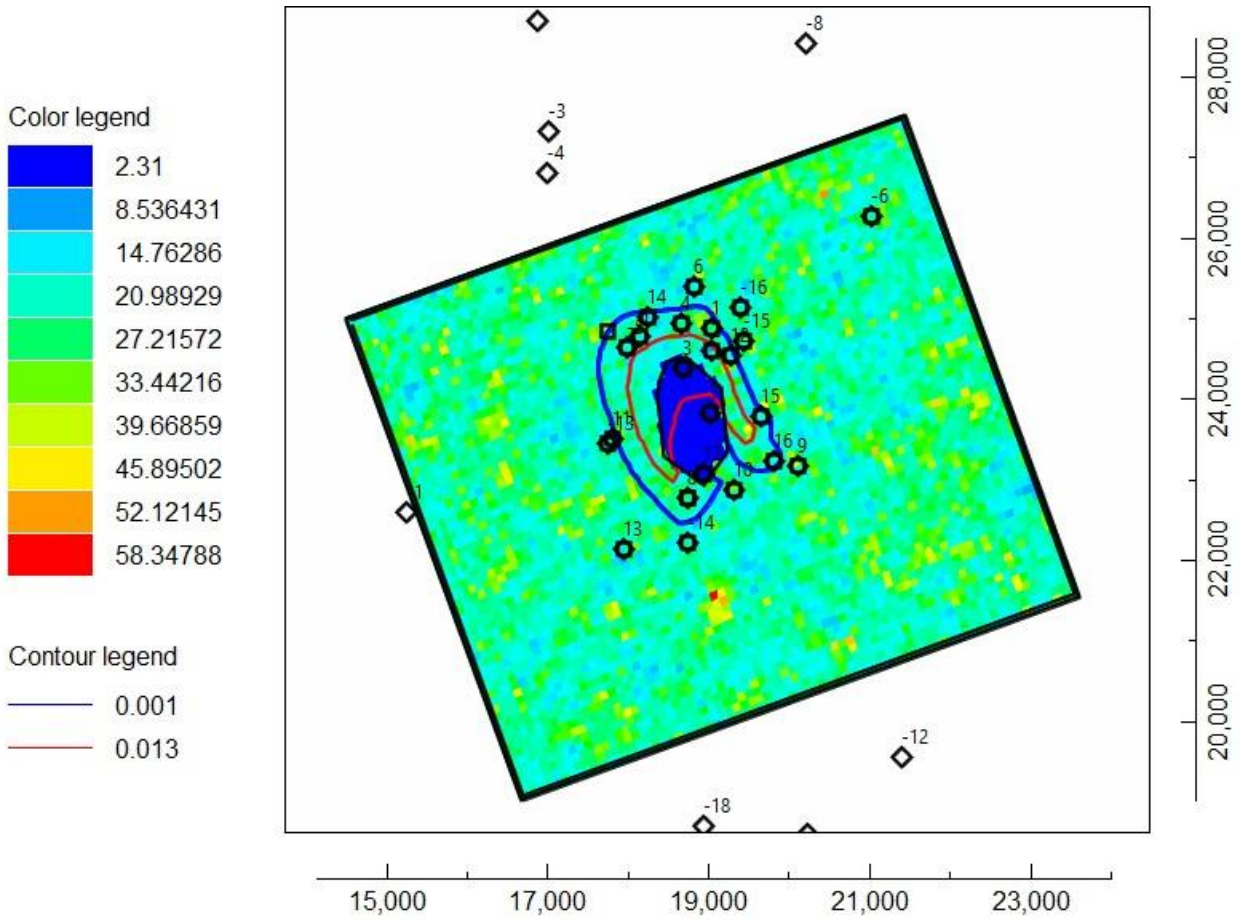

Figure 25. Concentration plume in layer 3 of hydraulic conductivity distribution A. The contours indicate concentration of MTBE in units of grams per cubic meter. The color legend indicates the hydraulic conductivity in the units of meters per day. The horizontal axis is the x spatial coordinate (m) and the vertical axis is the y spatial coordinate (m). Monitoring wells are denoted with a "-" sign.

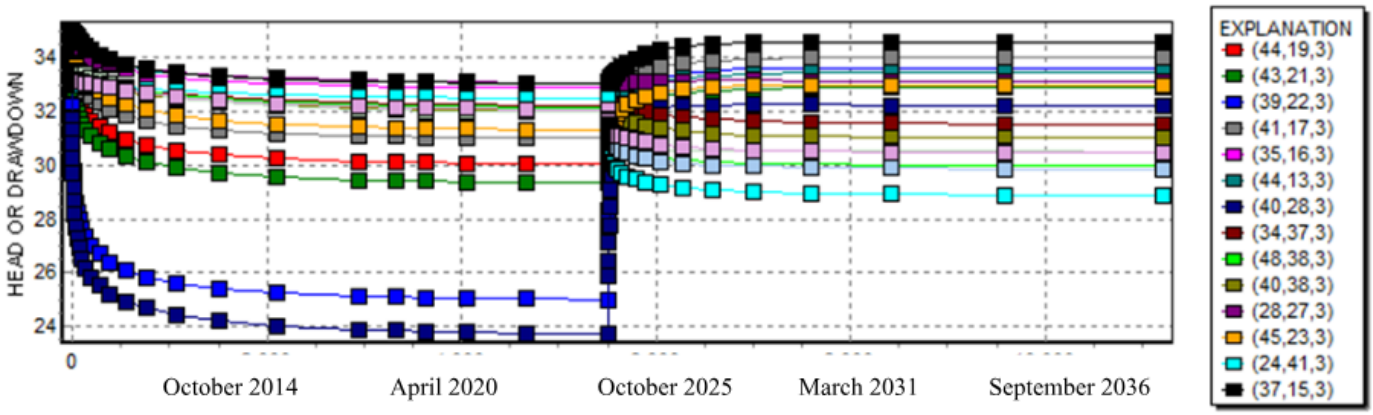

Figure 26. Head (m) (layer 3) versus date for all pumping wells with hydraulic conductivity distribution A. Refer to table 16 to interpret legend generated by GW_Chart.

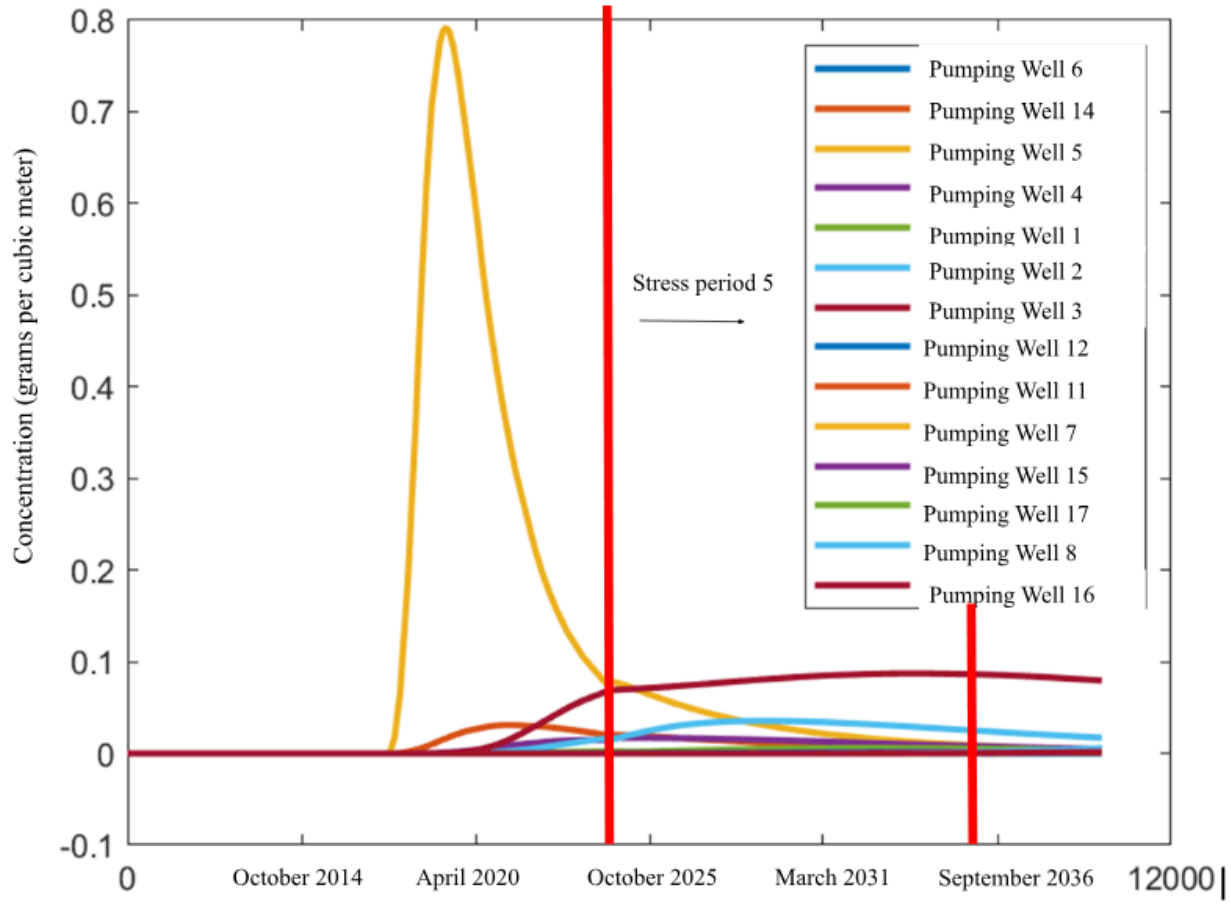

Figure 27. Breakthrough curve, showing only wells 5, 2, 3, 4, and 14 exceed the concentration for stress period 5. These wells are not pumping during this stress period.

Hydraulic Conductivity Distribution B

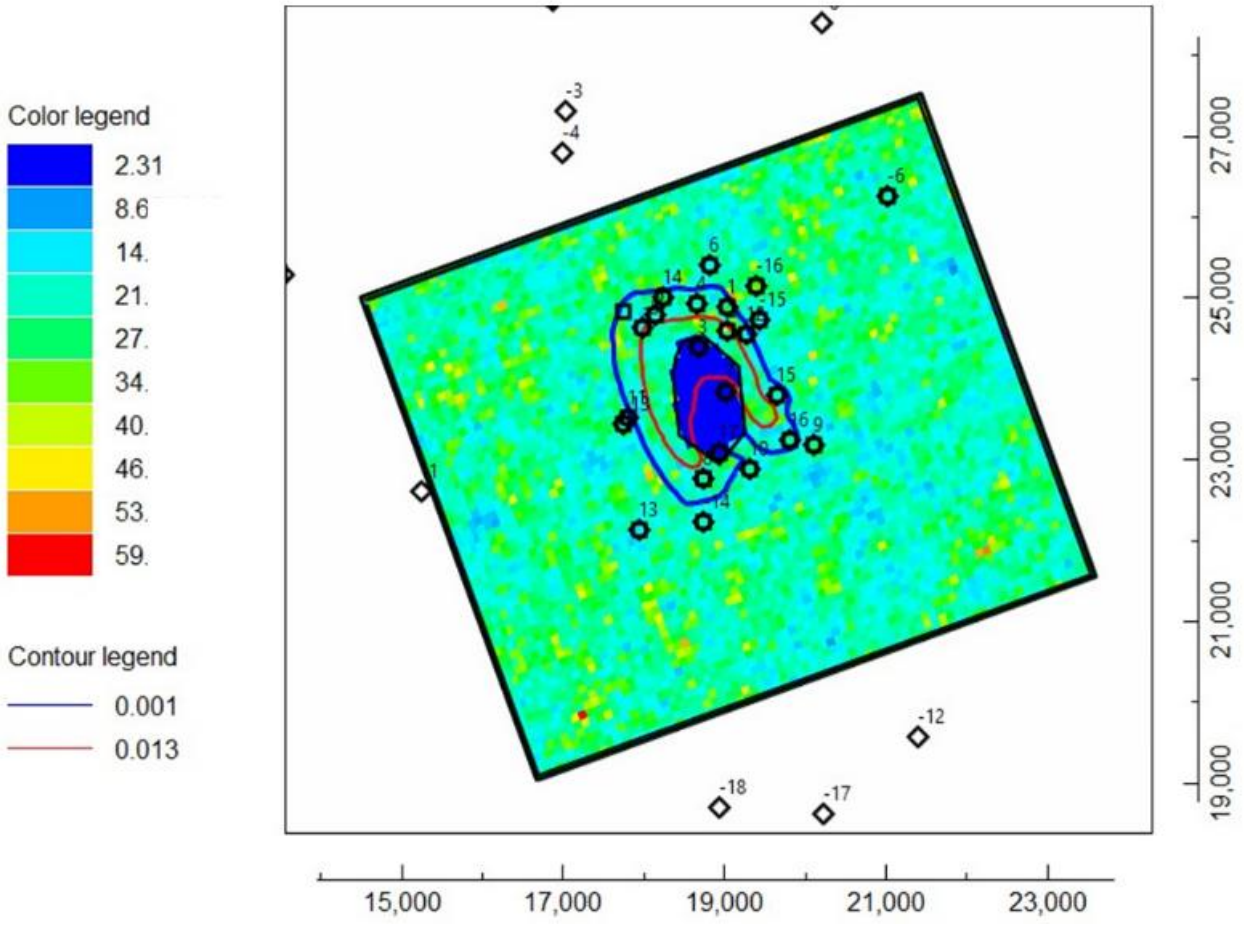

Figure 28. Hydraulic conductivity distribution and MTBE plume for hydraulic conductivity distribution B. The contours indicate concentration of MTBE in units of grams per cubic meter. The color legend indicates the hydraulic conductivity in the units of meters per day. The horizontal axis is the x spatial coordinate (m) and the vertical axis is the y spatial coordinate (m). Monitoring wells are denoted with a "-" sign.

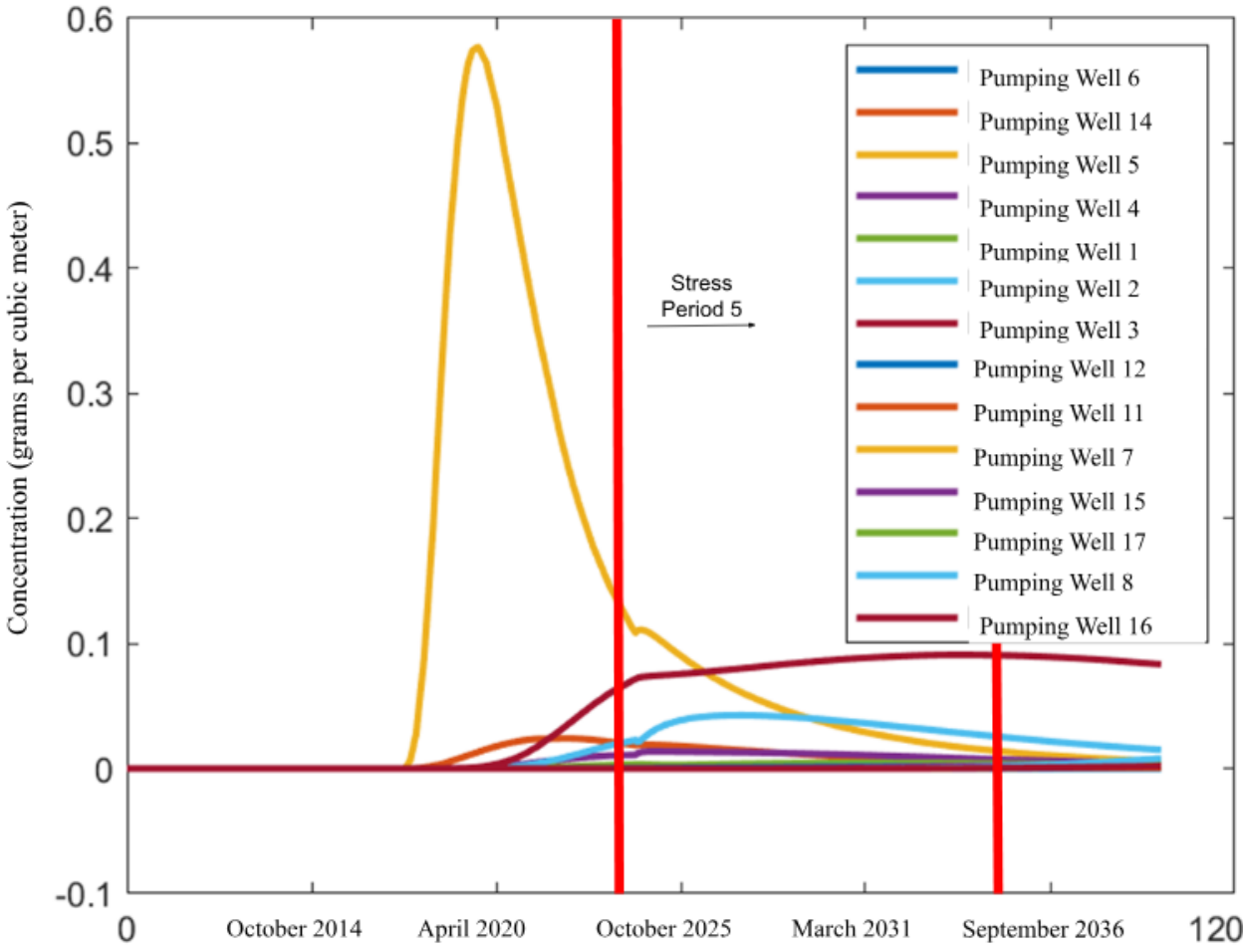

Figure 29. Breakthrough curve, showing only wells 5, 2, 3, 4, and 14 exceed the concentration for stress period 5. These wells are not pumping during this stress period.

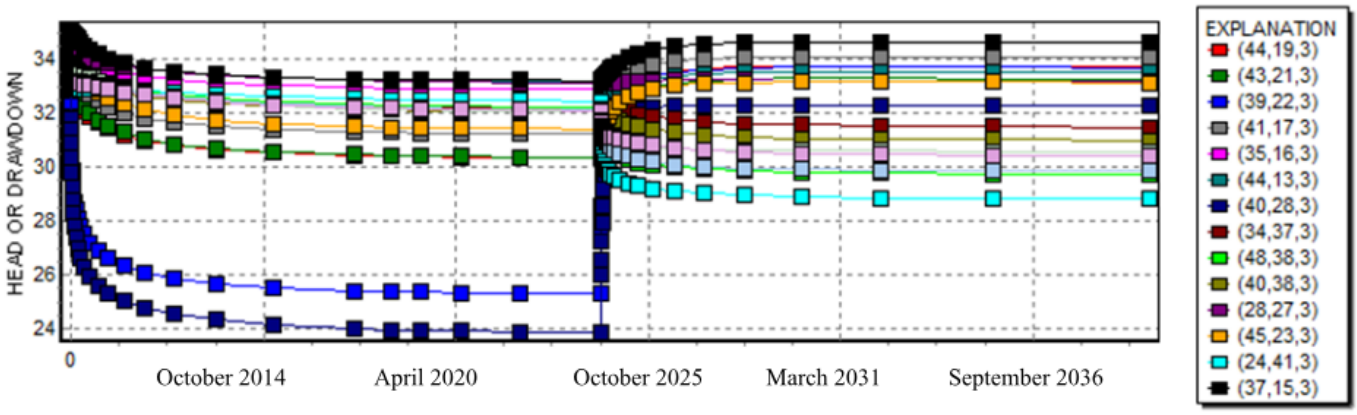

Figure 30. Head (m) (layer 3) versus date for all pumping wells with hydraulic conductivity distribution B. Refer to table 16 to interpret legend generated by GW_Chart.

Hydraulic Conductivity Distribution C

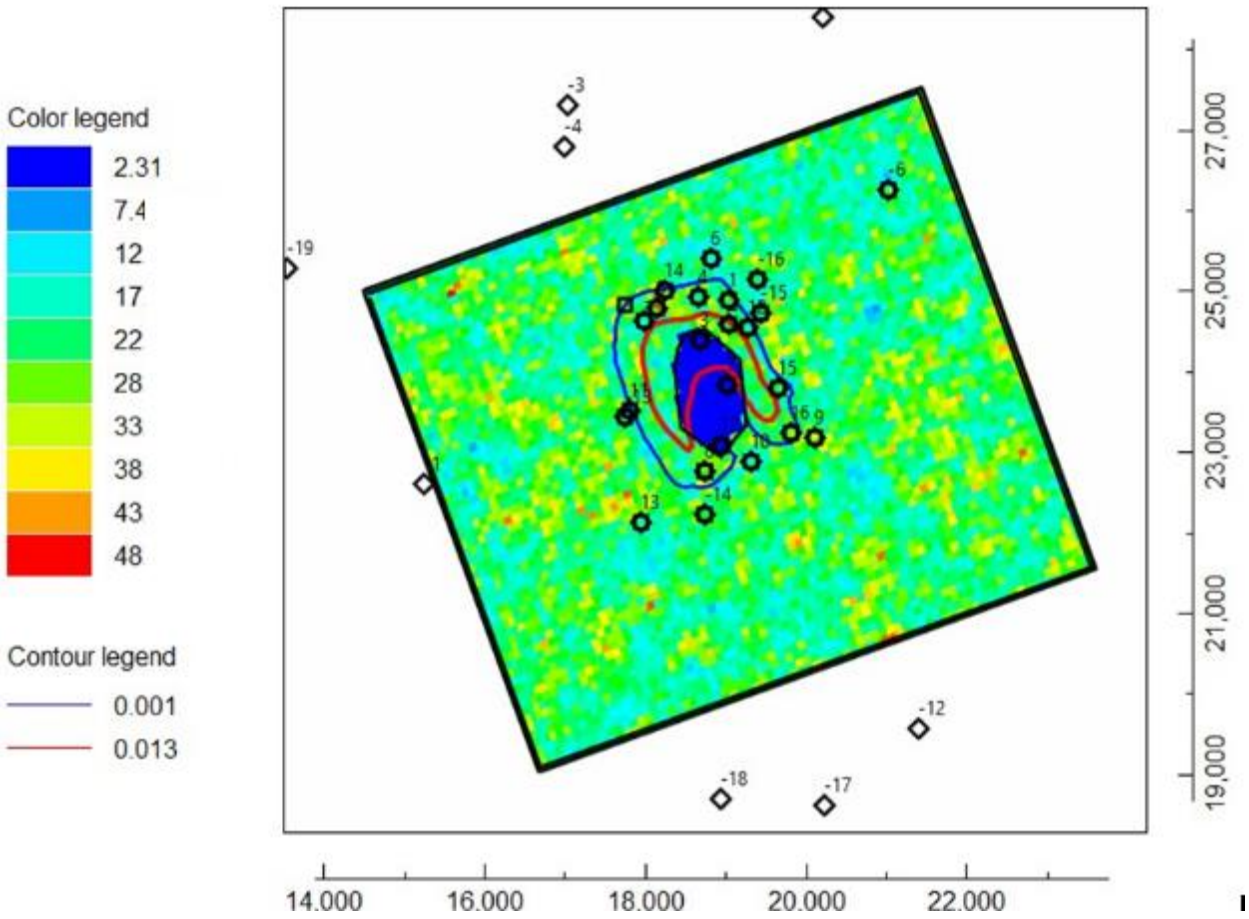

Figure 31. Hydraulic conductivity distribution and MTBE plume for hydraulic conductivity distribution C. The contours indicate concentration of MTBE in units of grams per cubic meter. The color legend indicates the hydraulic conductivity in the units of meters per day. The horizontal axis is the x spatial coordinate (m) and the vertical axis is the y spatial coordinate (m). Monitoring wells are denoted with a "-" sign.

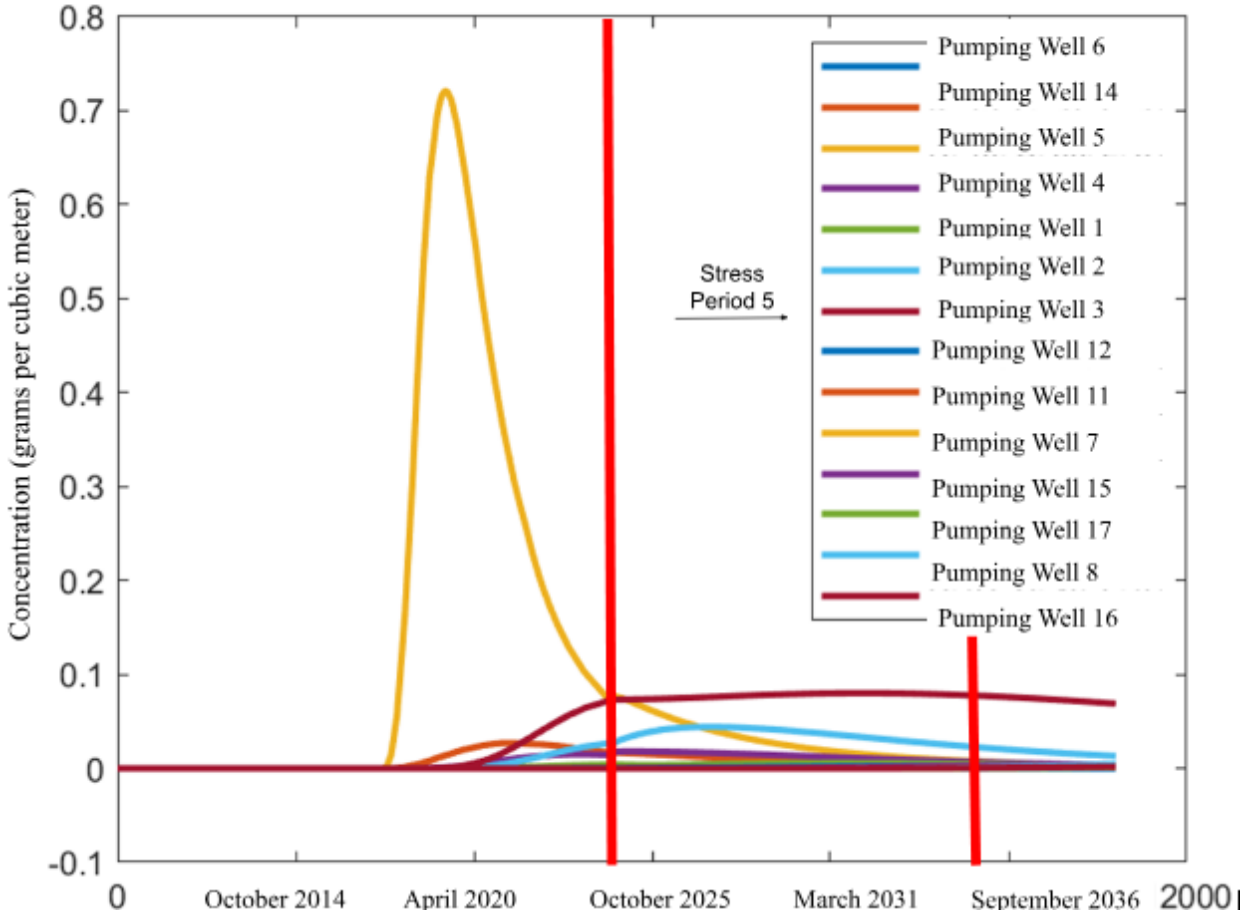

Figure 32. Breakthrough curve, showing only wells 5, 2, 3, 4, and 14 exceed the concentration for stress period 5. These wells are not pumping during this stress period.

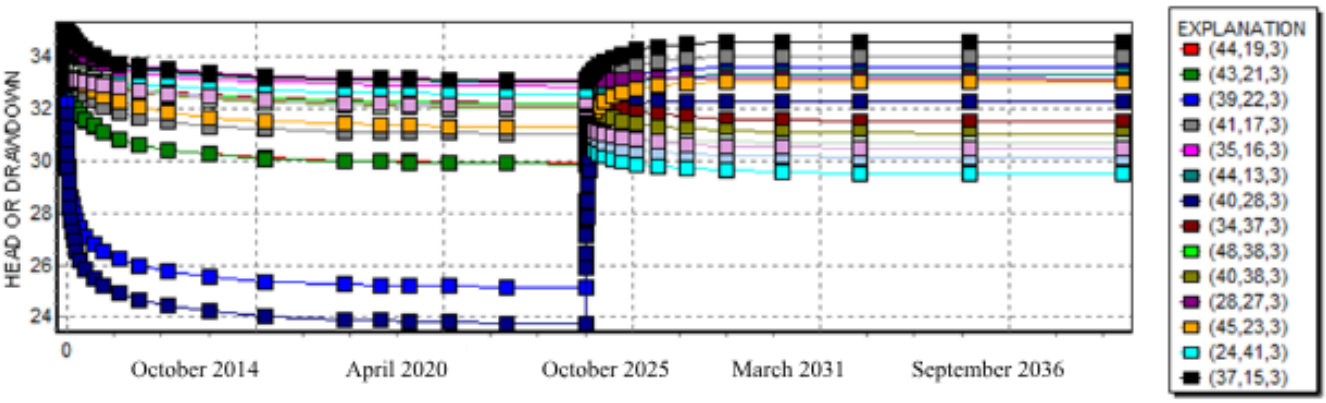

Figure 33. Head (m) (layer 3) versus date for all pumping wells with hydraulic conductivity distribution C. Refer to table 16 to interpret legend generated by GW_Chart.

Hydraulic Conductivity Distribution D

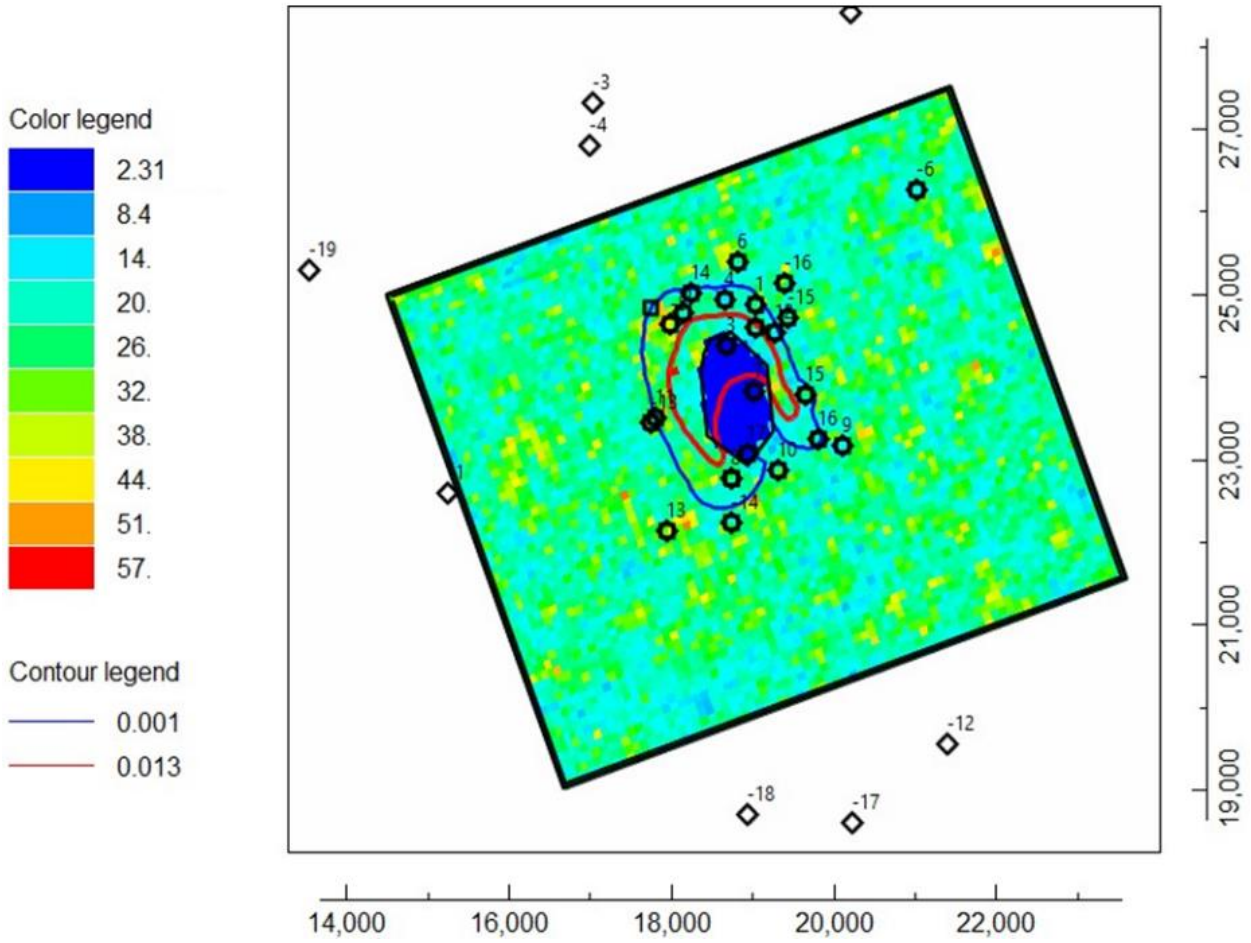

Figure 34. Hydraulic conductivity distribution and MTBE plume for hydraulic conductivity distribution D. The contours indicate concentration of MTBE in units of grams per cubic meter. The color legend indicates the hydraulic conductivity in the units of meters per day. The horizontal axis is the x spatial coordinate (m) and the vertical axis is the y spatial coordinate (m). Monitoring wells are denoted with a "-" sign.

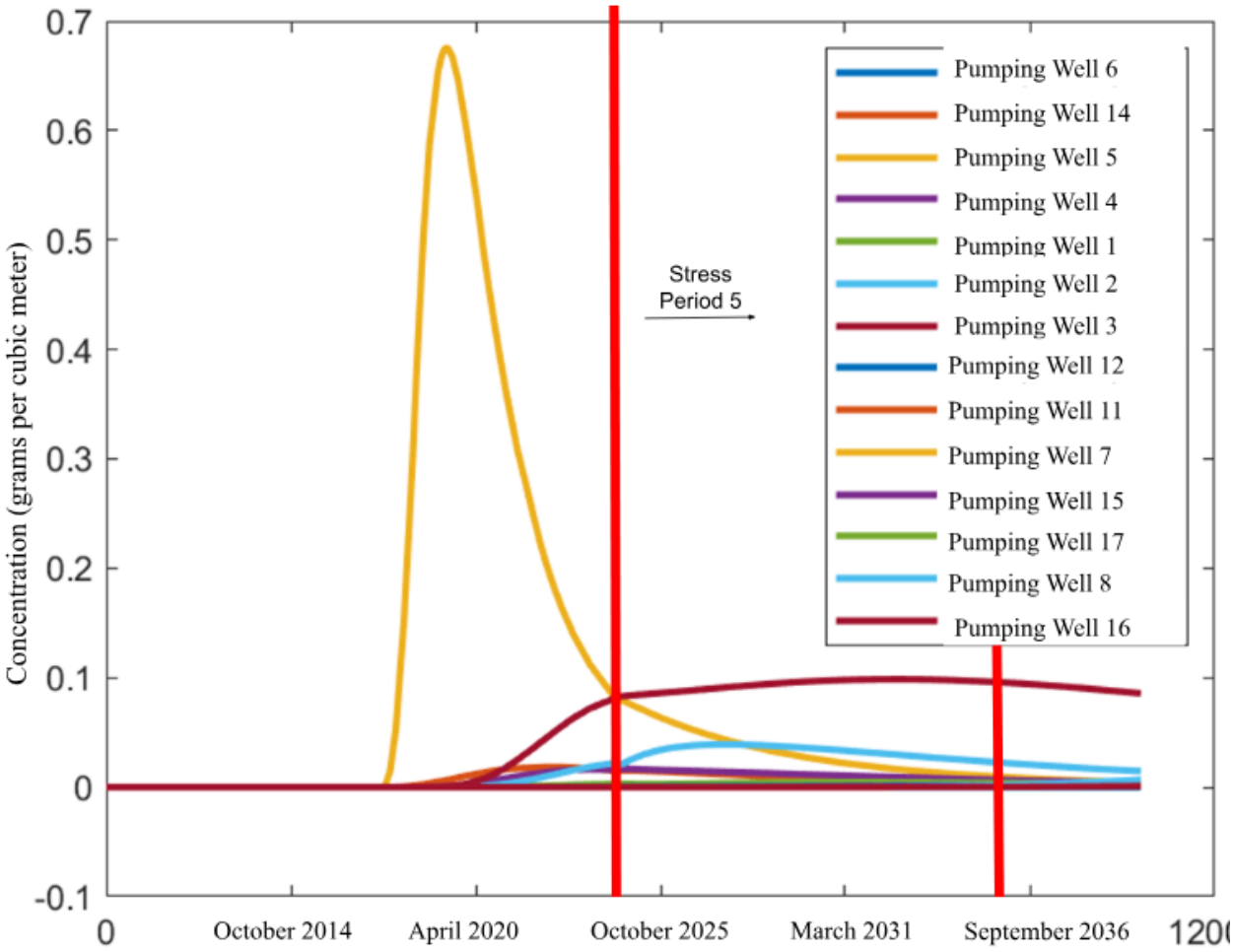

Figure 35. Breakthrough curve, showing only wells 5, 2, 3, 4, and 14 exceed the concentration for stress period 5. These wells are not pumping during this stress period.

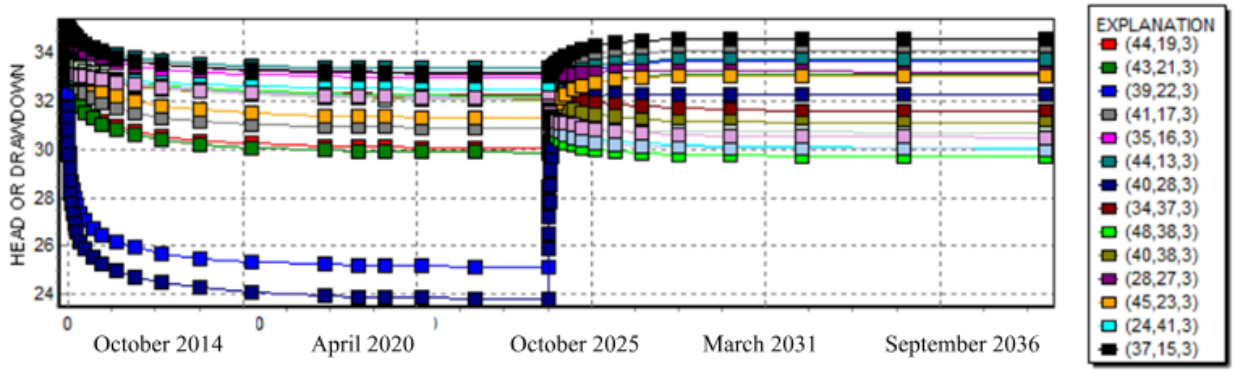

Figure 36. Head (m) (layer 3) versus date for all pumping wells with hydraulic conductivity distribution D. Refer to table 16 to interpret legend generated by GW_Chart.

Hydraulic Conductivity Distribution E

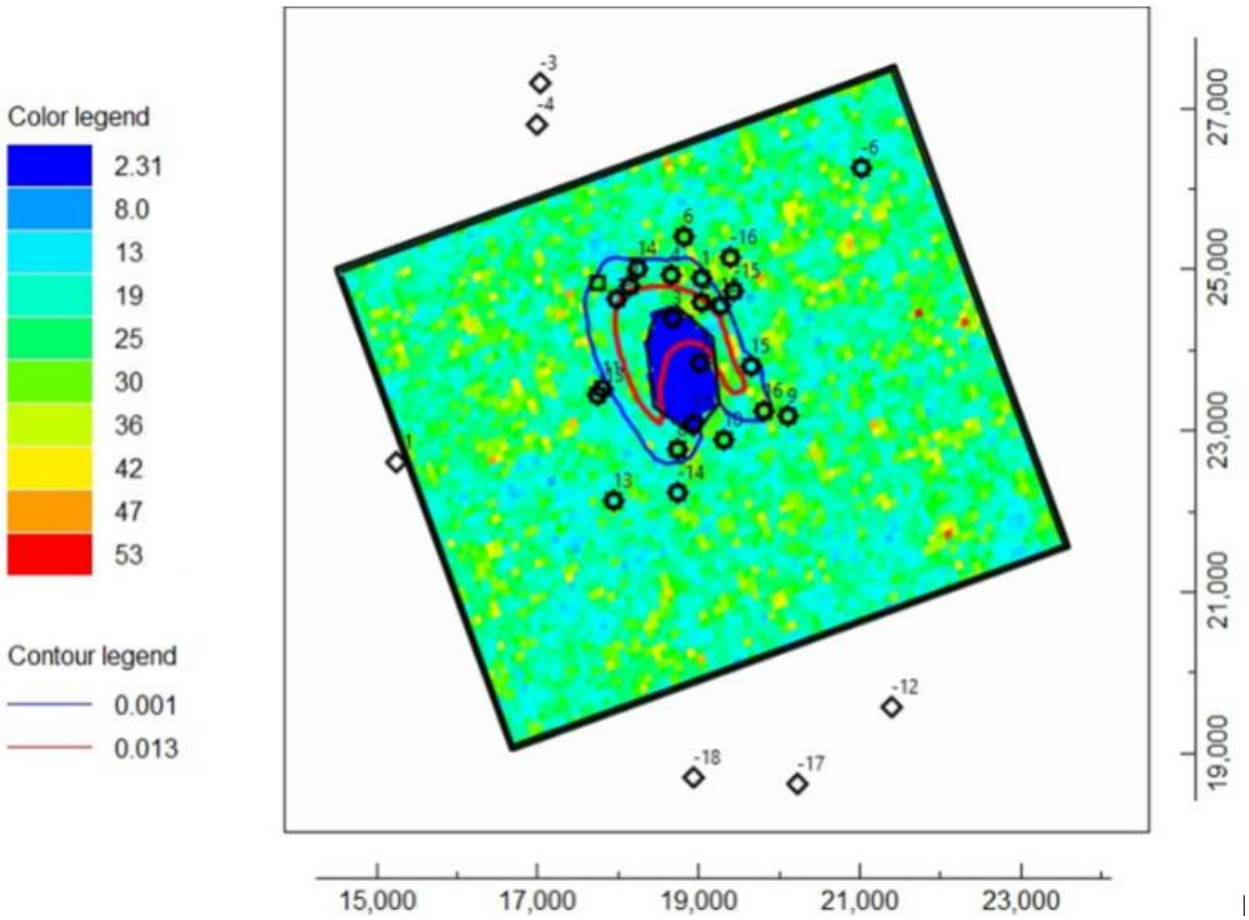

Figure 37. Hydraulic conductivity distribution and MTBE plume for hydraulic conductivity distribution E. The contours indicate concentration of MTBE in units of grams per cubic meter. The color legend indicates the hydraulic conductivity in the units of meters per day. The horizontal axis is the x spatial coordinate (m) and the vertical axis is the y spatial coordinate (m). Monitoring wells are denoted with a "-" sign.

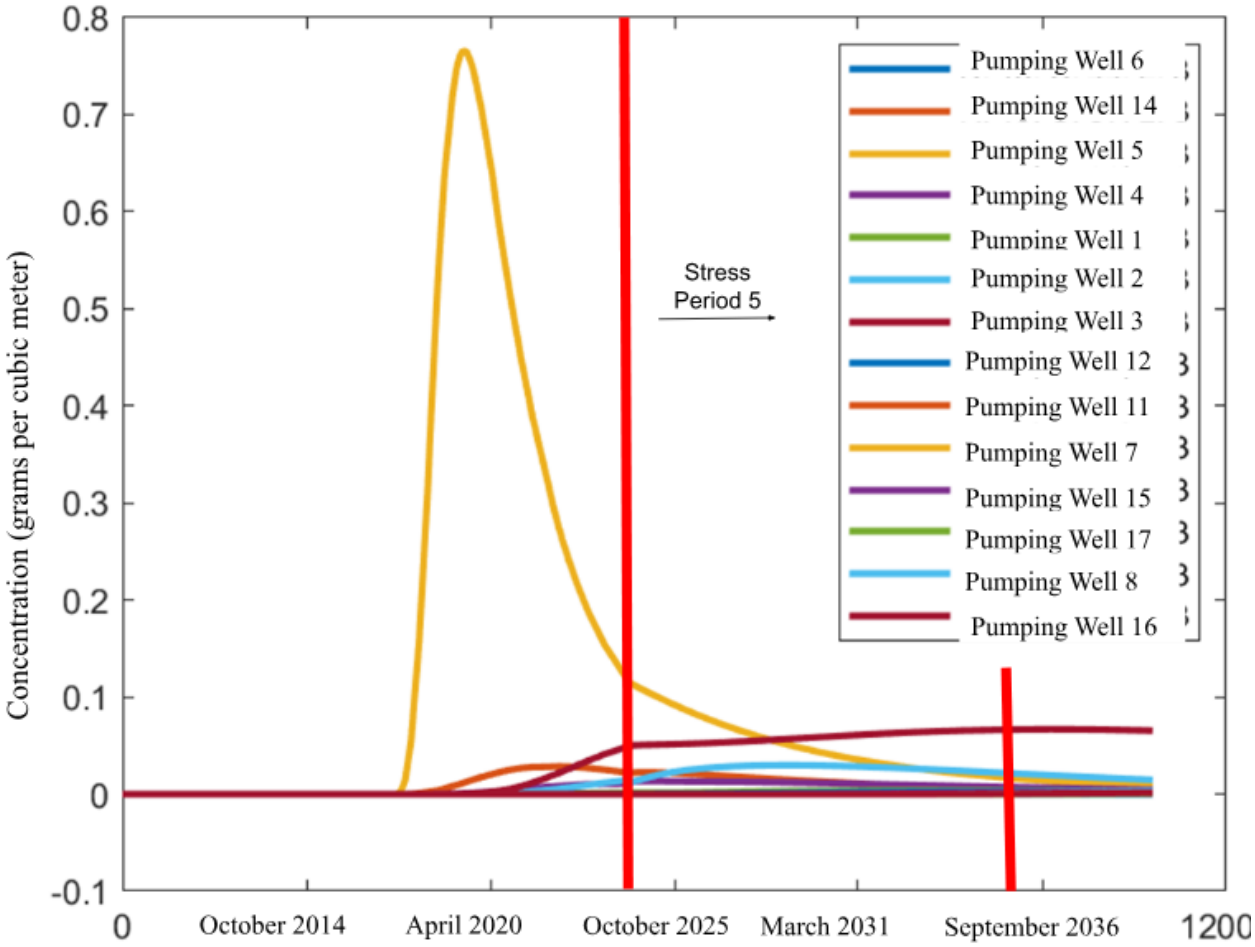

Figure 38. Breakthrough curve, showing only wells 5, 2, 3, 4, and 14 exceed the concentration for stress period 5. These wells are not pumping during this stress period.

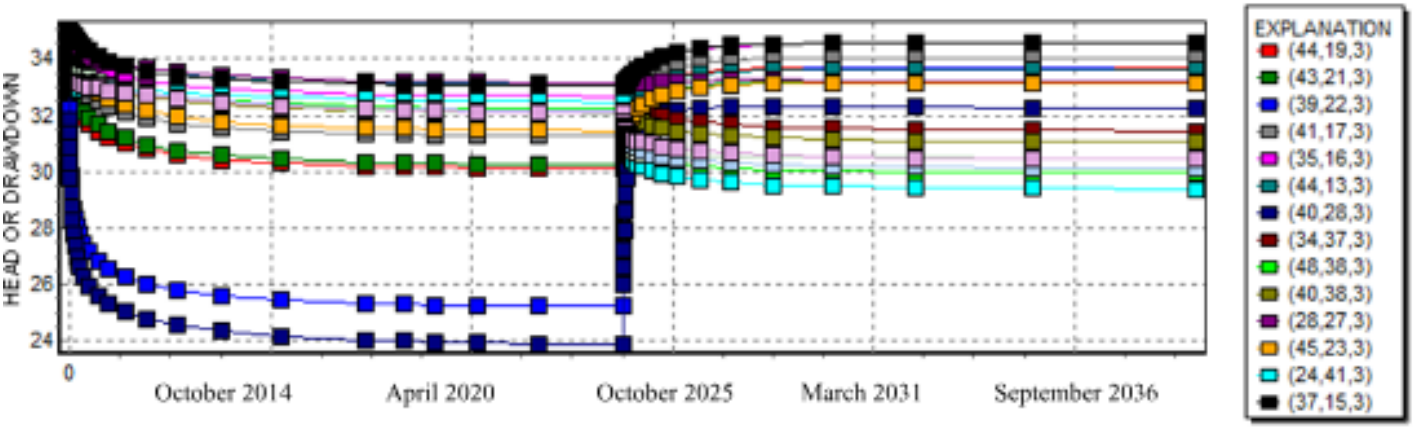

Figure 39. Head (m) (layer 3) versus date for all pumping wells with hydraulic conductivity distribution E. Refer to table 16 to interpret legend generated by GW_Chart.

Probability Analysis

As seen by the figures above, all five realizations of the hydraulic conductivity meet the requirements with the chosen pumping scheme. Concentration does not exceed the limit and no wells go dry. Therefore, the design is satisfactory for all realizations. The probability that the pumping scheme produces clean water is

$$\frac{\#\ of\ Realizations\ in\ which\ pumping\ scheme\ produced\ clean\ water}{Total\ \#\ of\ realizations} = \frac{5}{5} = 1$$

Of course, this is not a comprehensive probability analysis as only 5 realizations were generated with one value of standard deviation. However, this is satisfactory to demonstrate that the pumping scheme works for this aquifer.

Bibliography

Duffield, G. (2019, June 06). Aquifer testing 101: Hydraulic properties representative values of hydraulic properties. Retrieved from http://www.aqtesolv.com/aquifer-tests/aquifer_properties.htm

Johnson, A. I. (1976). Specific Yield -- Compilation of Specific Yields for Various Materials. In Hydrologic Properties of Earth Materials. essay, USGS.

Rawls et al. (1998). Saturated hydraulic conductivity for different soils. American Society of Agricultural and Biological Engineers.

WoIff, R. G. (1982). PHYSICAL PROPERTIES OF ROCKS POROSITY, PERMEABILITY, DISTRIBUTION COEFFICIENTS, AND DISPERSIVITY. United States Geological Survey.

Appendix A: Given Data: Tables and Figures

Table 1A. Measured heads in pumping wells at selected times

Well	Head (m)					
	4/30/2009	2/25/2010	1/9/2015	6/2/2018	4/16/2019	12/23/2023
1	33.12	31.82	30.83	30.58	30.53	30.32
2	34.25	31.56	30.55	30.30	30.25	30.03
3	34.50	22.23	20.78	20.34	20.23	19.89
4	34.83	32.86	31.89	31.64	31.59	31.39
5	35.08	33.78	32.86	32.62	32.57	32.37
6	35.29	34.30	33.41	33.17	33.12	32.93
7	33.88	32.61	31.76	31.53	31.48	31.28
8	33.32	33.00	32.34	32.12	32.07	31.88
9	33.29	33.11	32.48	32.26	32.22	32.03
10	33.23	33.00	32.33	32.11	32.07	31.88
11	34.06	33.78	33.03	32.80	32.75	32.56
12	34.21	33.36	32.47	32.23	32.18	31.98
13	33.05	32.96	32.45	32.26	32.22	32.04
14	35.16	34.17	33.24	33.01	32.96	32.76
15	33.80	33.39	32.61	32.38	32.33	32.14
16	33.39	33.15	32.47	32.25	32.21	32.02
17	33.46	33.14	32.42	32.20	32.15	31.96

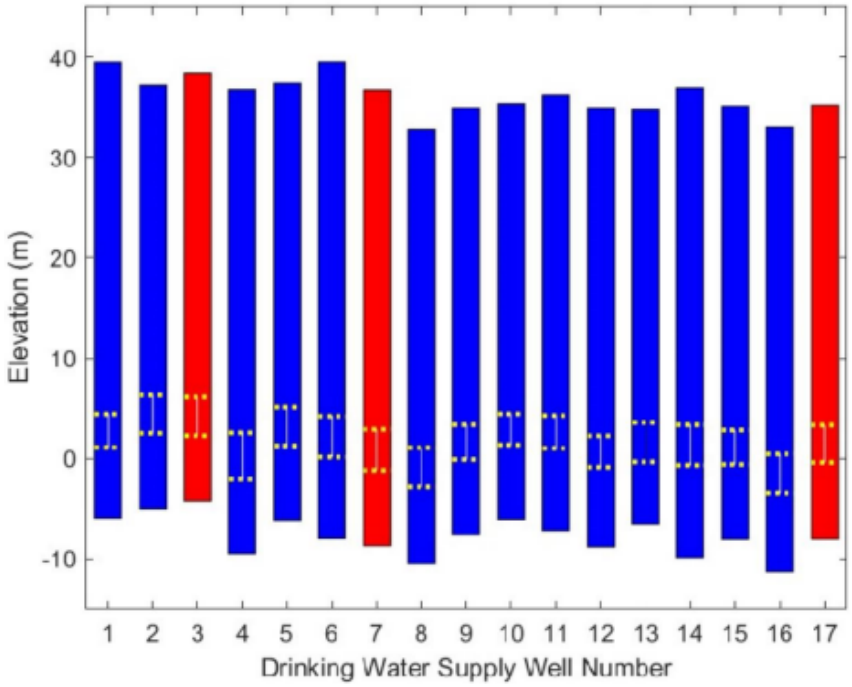

Figure 1A. Lithology of pumping wells. Vertical axes denotes elevation above sea level. Pumping well numbers are shown across the bottom. Blue shading represents medium sand and

red shading represents sandy loam. The screened interval is denoted by a thin vertical line. The top and bottom of the screened intervals are denoted by thick black lines.

Table 2A. Pumping well specifications

Well Number	x (m)	y (m)	Land Surface Elevation (m)	Top of Well Screen (m)	Bottom of Well Screen (m)	Elevation of Bedrock (m)	Pumping Rate (m^3/d)	Diameter (m)
1	19042	24881	39.49	4.44	1.10	-5.97	3120	0.5
2	19035	24597	37.17	6.30	2.52	-5.06	2120	0.5
3	18672	24384	38.43	6.12	2.26	-4.20	1460	0.5
4	18664	24932	36.76	2.56	-2.08	-9.48	1780	0.5
5	18145	24788	37.37	5.12	1.26	-6.17	980	0.5
6	18825	25399	39.50	4.23	0.14	-7.99	520	0.5
7	19008	23829	36.71	2.89	-1.17	-8.71	1470	0.5
8	18733	22774	32.83	1.08	-2.83	-10.50	180	0.5
9	20109	23175	34.91	3.36	-0.11	-7.61	0	0.5
10	19321	22876	35.39	4.45	1.35	-6.08	0	0.5
11	17814	23513	36.24	4.29	1.02	-7.16	215	0.5
12	19280	24543	34.88	2.25	-0.87	-8.81	0	0.5
13	17953	22136	34.75	3.59	-0.34	-6.52	0	0.5
14	18249	25013	36.91	3.35	-0.68	-9.86	0	0.5
15	19660	23790	35.14	2.82	-0.60	-8.07	0	0.5
16	19818	23241	33.06	0.44	-3.44	-11.30	0	0.5
17	18943	23076	35.24	3.32	-0.40	-8.05	0	0.5

Table 3A. 2009 heads used to determine boundary conditions

x (m)	y (m)	Well No.	Head (m) in 2009
19042	24881	1	33.12
19035	24597	2	34.25
18672	24384	3	34.50
18664	24932	4	34.83
18145	24788	5	35.08
18825	25399	6	35.29
19008	23829	7	33.88
18733	22774	8	33.32
20109	23175	9	33.29
19321	22876	10	33.23
17814	23513	11	34.06
19280	24543	12	34.21
17953	22136	13	33.05
18249	25013	14	35.16
19660	23790	15	33.80
19818	23241	16	33.39
18943	23076	17	33.46
15249	22603	-1	34.41
14706	29573	-2	40.15
17022	27313	-3	37.81
16984	26796	-4	37.38
17977	24635	-5	35.04
21015	26267	-6	35.86

x (m)	y (m)	Well No.	Head (m) in 2009
16870	28681	-7	38.98
20207	28406	-8	37.93
26708	25041	-9	33.63
26688	23085	-10	31.70
25937	21012	-11	29.83
21403	19565	-12	29.63
17746	23449	-13	34.15
18741	22230	-14	32.87
19442	24721	-15	34.37
19402	25143	-16	34.74
20232	18613	-17	28.98
18945	18703	-18	29.57
13544	25292	-19	37.20
11175	21660	-20	34.90
14596	17501	-21	29.82
18439	14659	-22	24.99
24703	16133	-23	24.40
26914	29555	-24	37.46
20913	32345	-25	40.78
13859	31292	-26	41.53
12228	31924	-27	42.29
9595	27713	-28	40.06

Pumping Well Specifications

Table 4A. Measured heads in monitoring wells at selected times

Well	Head (m)					
	4/30/2009	2/25/2010	1/9/2015	6/2/2018	4/16/2019	12/23/2023
1	34.41	34.40	34.13	33.98	33.94	33.79
2	40.15	40.15	40.06	39.98	39.96	39.87
3	37.81	37.77	37.38	37.22	37.18	37.03
4	37.38	37.32	36.86	36.69	36.65	36.49
5	35.04	34.28	33.39	33.16	33.11	32.91
6	35.86	35.81	35.35	35.16	35.12	34.95
7	38.98	38.97	38.76	38.63	38.60	38.47
8	37.93	37.92	37.66	37.52	37.48	37.34
9	33.63	33.63	33.58	33.52	33.50	33.42
10	31.70	31.70	31.65	31.59	31.58	31.49
11	29.83	29.83	29.78	29.72	29.70	29.62
12	29.63	29.63	29.49	29.38	29.35	29.23
13	34.15	33.89	33.16	32.93	32.89	32.70
14	32.87	32.75	32.19	31.99	31.94	31.76
15	34.37	33.62	32.74	32.50	32.45	32.25
16	34.74	34.05	33.17	32.94	32.89	32.69
17	28.98	28.98	28.87	28.78	28.75	28.63
18	29.57	29.57	29.45	29.34	29.31	29.19
19	37.20	37.20	37.05	36.94	36.91	36.79
20	34.90	34.90	34.86	34.81	34.79	34.72
21	29.82	29.82	29.77	29.72	29.70	29.62
22	24.99	24.99	24.98	24.95	24.94	24.89
23	24.40	24.40	24.39	24.36	24.36	24.31
24	37.46	37.46	37.44	37.40	37.39	37.33
25	40.78	40.78	40.74	40.69	40.67	40.60
26	41.53	41.53	41.50	41.45	41.44	41.38
27	42.29	42.29	42.28	42.25	42.24	42.20
28	40.06	40.06	40.05	40.02	40.01	39.96

Table 5A. Measured concentrations at all pumping wells and monitoring wells where MTBE was detected**.**

	Concentration (mg/L)					
Date	Well 2	Well 3	Well 4	Well 5	Well 14	MW 5
12/1/2017	0.0000	0.0000	0.0000	0.0038	0.0000	0.0035
3/1/2018	0.0000	0.0000	0.0000	0.0267	0.0000	0.0312
6/1/2018	0.0000	0.0000	0.0000	0.0868	0.0000	0.1146
9/1/2018	0.0000	0.0000	0.0000	0.1881	0.0000	0.2658
12/1/2018	0.0000	0.0000	0.0000	0.3175	0.0000	0.4690
3/1/2019	0.0000	0.0000	0.0000	0.4462	0.0000	0.6811
6/1/2019	0.0000	0.0000	0.0000	0.5502	0.0000	0.8597
9/1/2019	0.0000	0.0000	0.0000	0.6157	0.0000	0.9761
12/1/2019	0.0000	0.0000	0.0000	0.6429	0.0000	1.0278
3/1/2020	0.0000	0.0000	0.0000	0.6401	0.0000	1.0284
6/1/2020	0.0000	0.0016	0.0000	0.6156	0.0000	0.9925
9/1/2020	0.0000	0.0031	0.0000	0.5776	0.0013	0.9341
12/1/2020	0.0000	0.0056	0.0000	0.5329	0.0020	0.8646
3/1/2021	0.0000	0.0092	0.0000	0.4855	0.0027	0.7904
6/1/2021	0.0000	0.0143	0.0000	0.4373	0.0035	0.7148
9/1/2021	0.0014	0.0208	0.0000	0.3910	0.0042	0.6420
12/1/2021	0.0022	0.0285	0.0000	0.3482	0.0049	0.5746
3/1/2022	0.0032	0.0373	0.0000	0.3094	0.0056	0.5133
6/1/2022	0.0047	0.0473	0.0000	0.2729	0.0061	0.4553
9/1/2022	0.0064	0.0577	0.0000	0.2407	0.0066	0.4040
12/1/2022	0.0085	0.0684	0.0010	0.2116	0.0069	0.3573
3/1/2023	0.0107	0.0787	0.0012	0.1865	0.0071	0.3168
6/1/2023	0.0133	0.0888	0.0015	0.1636	0.0073	0.2797
9/1/2023	0.0159	0.0981	0.0017	0.1434	0.0073	0.2468
12/1/2023	0.0186	0.1064	0.0019	0.1259	0.0073	0.2181

Table 6A. Monitoring well Specifications

Well Number	x (m)	y (m)	Land Surface Elevation (m)	Top of Well Screen (m)	Bottom of Well Screen (m)	Elevation of Bedrock (m)	Pumping Rate (m^3/d)	Diameter (m)
1	15249	22603	37.20	8.14	4.18	-3.94	0	0.1
2	14706	29573	41.26	7.48	2.34	-6.50	0	0.1
3	17022	27313	38.39	5.51	0.36	-7.85	0	0.1
4	16984	26796	36.35	3.25	-1.13	-9.42	0	0.1
5	17977	24635	37.12	2.24	-1.91	-10.53	0	0.1
6	21015	26267	37.34	2.24	-2.61	-10.38	0	0.1
7	16870	28681	41.61	9.90	5.96	-3.69	0	0.1
8	20207	28406	40.08	5.67	2.19	-5.80	0	0.1
9	26708	25041	34.80	6.05	2.44	-4.46	0	0.1
10	26688	23085	31.62	1.01	-1.80	-9.58	0	0.1
11	25937	21012	29.64	-0.39	-4.23	-9.90	0	0.1
12	21403	19565	31.25	1.27	-2.16	-8.37	0	0.1
13	17746	23449	35.75	3.33	0.16	-7.50	0	0.1
14	18741	22230	33.77	4.15	0.90	-5.96	0	0.1
15	19442	24721	36.28	3.49	0.03	-9.55	0	0.1
16	19402	25143	35.57	1.40	-2.20	-10.18	0	0.1
17	20232	18613	30.93	0.87	-2.57	-8.71	0	0.1
18	18945	18703	31.76	1.82	-1.46	-8.45	0	0.1
19	13544	25292	39.01	5.20	1.47	-5.94	0	0.1
20	11175	21660	36.80	1.65	-2.35	-9.02	0	0.1
21	14596	17501	29.08	-1.39	-4.54	-10.21	0	0.1
22	18439	14659	28.76	2.83	-0.23	-5.62	0	0.1
23	24703	16133	28.01	-0.68	-3.83	-8.60	0	0.1
24	26914	29555	37.47	1.61	-2.60	-11.45	0	0.1
25	20913	32345	41.96	7.18	3.10	-6.39	0	0.1
26	13859	31292	45.54	8.47	4.05	-4.42	0	0.1
27	12228	31924	46.42	7.75	3.61	-3.79	0	0.1
28	9595	27713	42.72	9.88	5.27	-3.22	0	0.1

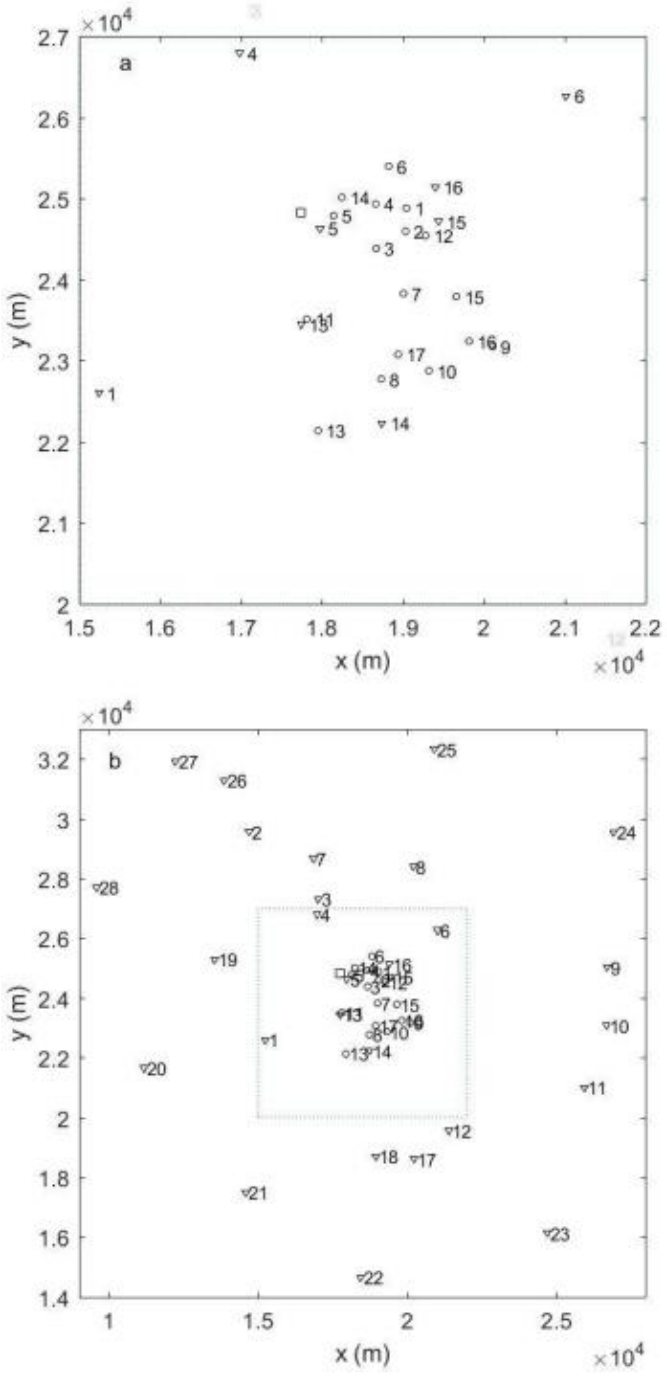

Figure 2A. Plan view of (a) site area and (b) entire region. The circles denote drinking water supply well locations, and the numbers correspond to the well number. The inverted triangles denote regional monitoring well locations, and the numbers correspond to the well number. The square (at x=17740 m, y=24830 m) is the location of the gas station that is the source of contamination. In this map, North is in the positive y direction. The dashed square in subplot b shows the extent of the plot domain in subplot a

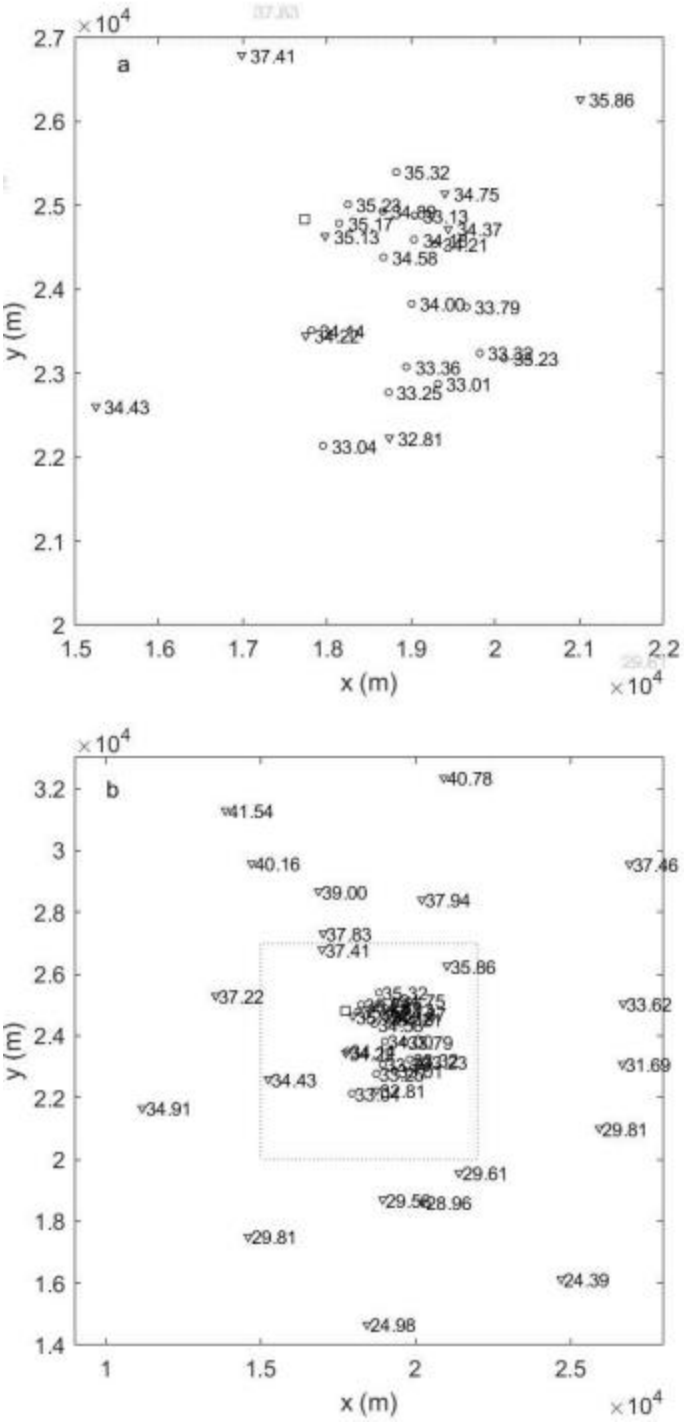

Figure 3A. Head (m) at each pumping well and monitoring well in 2009 in (a) site area and (b) entire region. The dashed square in subplot b shows the extent of the plot domain in subplot a. The square (at x=17740 m, y=24830 m) is the location of the gas station that is the source of contamination

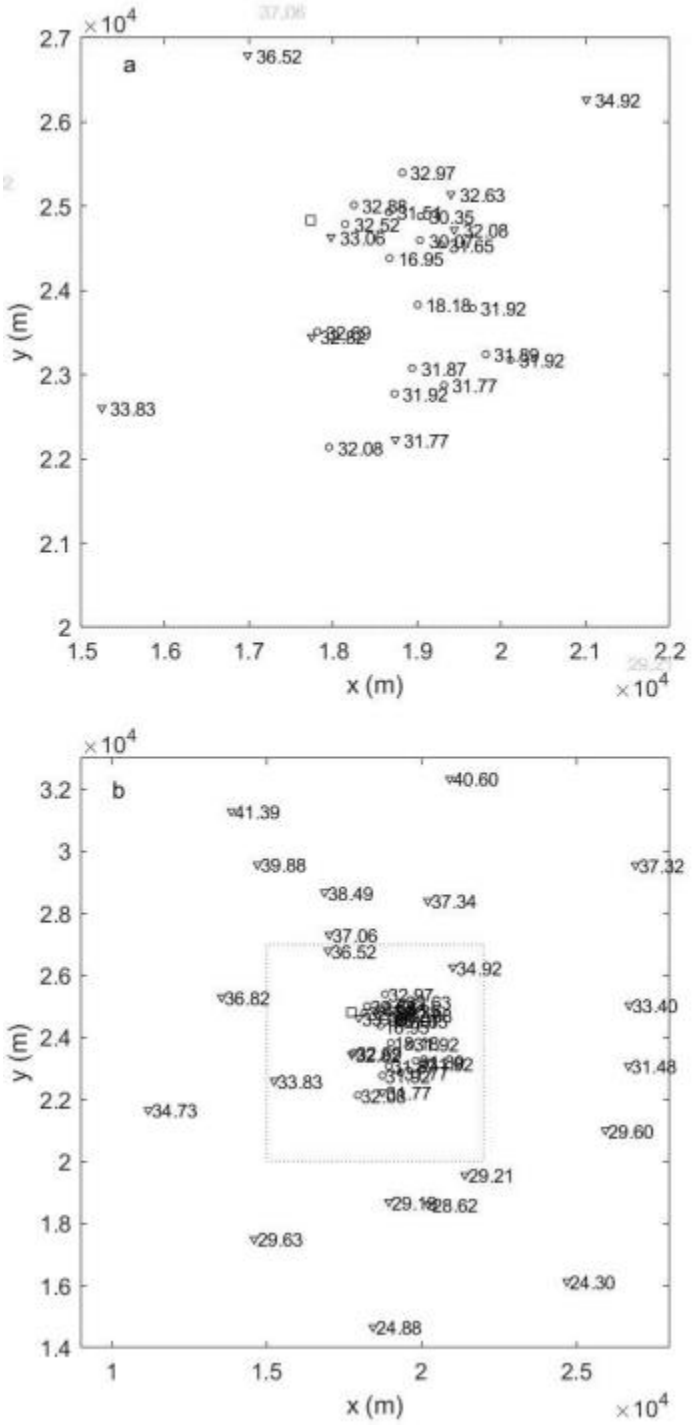

Figure 4A. Head (m) at each pumping well and monitoring well in December 2023 in (a) site area and (b) entire region. The dashed square in subplot b shows the extent of the plot domain in subplot a. The square (at x=17740 m, y=24830 m) is the location of the gas station that is the source of contamination.

Appendix B: Data Used in Model, Not Directly Referenced in Report

Table B1. Additional well information

	x (m)	y (m)	Well No.	Head (m) in 2009	Head (m) in 2023
1	19042	24881	1	33.12	30.32
2	19035	24597	2	34.25	30.03
3	18672	24384	3	34.50	19.89
4	18664	24932	4	34.83	31.39
5	18145	24788	5	35.08	32.37
6	18825	25399	6	35.29	32.93
7	19008	23829	7	33.88	31.28
8	18733	22774	8	33.32	31.88
9	20109	23175	9	33.29	32.03
10	19321	22876	10	33.23	31.88
11	17814	23513	11	34.06	32.56
12	19280	24543	12	34.21	31.98
13	17953	22136	13	33.05	32.04
14	18249	25013	14	35.16	32.76
15	19660	23790	15	33.80	32.14
16	19818	23241	16	33.39	32.02
17	18943	23076	17	33.46	31.96
18	15249	22603	-1	34.41	33.79
19	14706	29573	-2	40.15	39.87
20	17022	27313	-3	37.81	37.03
21	16984	26796	-4	37.38	36.49
22	17977	24635	-5	35.04	32.91
23	21015	26267	-6	35.86	34.95
24	16870	28681	-7	38.98	38.47
25	20207	28406	-8	37.93	37.34
26	26708	25041	-9	33.63	33.42
27	26688	23085	-10	31.70	31.49
28	25937	21012	-11	29.83	29.62
29	21403	19565	-12	29.63	29.23
30	17746	23449	-13	34.15	32.70
31	18741	22230	-14	32.87	31.76
32	19442	24721	-15	34.37	32.25
33	19402	25143	-16	34.74	32.69
34	20232	18613	-17	28.98	28.63
35	18945	18703	-18	29.57	29.19
36	13544	25292	-19	37.20	36.79
37	11175	21660	-20	34.90	34.72
38	14596	17501	-21	29.82	29.62
39	18439	14659	-22	24.99	24.89
40	24703	16133	-23	24.40	24.31
41	26914	29555	-24	37.46	37.33
42	20913	32345	-25	40.78	40.60
43	13859	31292	-26	41.53	41.38
44	12228	31924	-27	42.29	42.20
45	9595	27713	-28	40.06	39.96